Oscillatory calcium release and sustained store-operated oscillatory calcium signaling prevents differentiation of human oligodendrocyte progenitor cells

Richard A. Seidman[1], Heba Khattab[2], Jessie J. Polanco[1], Jacqueline E. Broome[2], Fraser J. Sim[1,2]

Neuroscience Program[1], Department of Pharmacology and Toxicology[2], Jacobs School of Medicine and Biomedical Sciences, University at Buffalo, Buffalo, NY.

Address correspondence to:

Fraser Sim, Ph.D.
Department of Pharmacology and Toxicology
Jacob's School of Medicine and Biomedical Sciences
University at Buffalo
955 Main Street
Buffalo, NY 14203
716-829-2151
fjsim@buffalo.edu

Keywords: human, lentivirus, STIM1, STIM2, muscarinic receptor, metabotropic glutamate receptor

Running title: STIM-dependent Ca-signaling blocks hOPC differentiation.

Abstract, 300 words; Introduction, 920 words; Discussion, 1518 words.

Figures: 5; Table: 1

Acknowledgements:

This work was supported by NINDS grant (R01NS104021), National Multiple Sclerosis Society (RG 5505-A-2, RG 5110A1/1), the Kalec Multiple Sclerosis Foundation, the Change MS Foundation, and the Skarlow Memorial Trust. JJP received support from NIGMS (R25GM09545902), NCATS (UL1TR001412-S1). JJP and RAS received support from NYSTEM Stem Cells in Regenerative Medicine Fellowship (#C302090G). We acknowledge the assistance of the Confocal Microscope and Flow Cytometry Facility in the School of Medicine and Biomedical Sciences, University at Buffalo. We thank Dr. Pablo Paez for advice with calcium imaging of OPCs.

ABSTRACT

Endogenous remyelination in demyelinating diseases such as multiple sclerosis is contingent upon the successful differentiation of oligodendrocyte progenitor cells (OPCs). Signaling via the $G\alpha_q$-coupled muscarinic receptor ($M_{1/3}R$) inhibits human OPC differentiation and impairs endogenous remyelination in experimental models. We hypothesized that calcium release following $G\alpha_q$-coupled receptor (G_qR) activation directly regulates human OPC (hOPC) cell fate. In this study, we show that specific G_qR agonists activating muscarinic and metabotropic glutamate receptors induce characteristic oscillatory calcium release in hOPCs and that these agonists similarly block hOPC maturation *in vitro*. Both agonists induce calcium release from ER stores and store operated calcium entry (SOCE) likely via STIM/ORAI-based channels. siRNA mediated knockdown (KD) of obligate calcium sensors STIM1 and STIM2 decreased the magnitude of muscarinic agonist induced oscillatory calcium release and attenuated SOCE in hOPCs. In addition, STIM2 expression was necessary to maintain the frequency of calcium oscillations and STIM2 KD reduced spontaneous OPC differentiation. Furthermore, STIM2 siRNA prevented the effects of muscarinic agonist treatment on OPC differentiation suggesting that SOCE is necessary for the anti-differentiative action of muscarinic receptor-dependent signaling. Finally, using a gain-of-function approach with an optogenetic STIM lentivirus, we demonstrate that independent activation of SOCE was sufficient to significantly block hOPC differentiation and this occurred in a frequency dependent manner while increasing hOPC proliferation. These findings suggest that intracellular calcium oscillations directly regulate hOPC fate and that modulation of calcium oscillation frequency may overcome inhibitory G_q-coupled signaling that impairs myelin repair.

Significance Statement

In this study, Seidman et al. show that SOCE is a common component of ligand-based $G\alpha_q$-coupled signaling in hOPCs and that SOCE alone is sufficient to block hOPC differentiation and drive proliferation. Therefore, SOCE blocks differentiation and that pathological SOCE could contribute to myelin disease.

INTRODUCTION

Efficient CNS remyelination is contingent upon successful intercellular signaling between neurons and glia that together orchestrate the processes of oligodendrocyte progenitor cell (OPC) recruitment, differentiation, and maturation into myelin-forming oligodendrocytes (OL) [1]. In demyelinating diseases such as multiple sclerosis (MS), the pathological environment contributes to an inhibition of OPC differentiation that limits remyelination and may contribute to subsequent permanent neurodegeneration [2]. In support of this hypothesis, numerous quiescent OPCs are observed in chronic MS lesions that appear to be unable to undergo OL differentiation [3,4]. Following demyelination, OPCs are exposed to a complex cellular microenvironment comprising extracellular matrix and soluble factors released by a variety of sources include infiltrating immune cells, reactive glia, and endothelial cells as well as injured axons that release both soluble growth factors and neurotransmitters. Neurotransmitters activate multiple and functionally distinct receptors expressed on OPCs and OLs that may contribute to activity-dependent or so-called adaptive myelination reviewed in [5]. Following demyelination, neuronal activity promotes remyelination [6] and this is regulated in part by AMPA and NMDA receptor signaling [7]. Intracellular calcium represents a common target for these activity-dependent pathways and a diverse set of neurotransmitters can induce intracellular calcium increase in glial progenitors [8].

Intracellular calcium release occurs in OPCs follows activation of ionotropic voltage and ligand gated channels and/or following activation of metabotropic receptors [9]. Muscarinic acetylcholine receptors M_1 and M_3 are $G\alpha_q$-coupled receptors that cause intracellular calcium release via PLCβ and inositol trisphosphate (IP_3) second messengers [10]. Genetic deletion of M_1/M_3 receptors in OPCs delays differentiation and remyelination in animal models of experimental demyelination [11,12]. Pharmacological inhibition of muscarinic receptors results in accelerated OL differentiation and remyelination in the brain and spinal cord following both toxin-induced demyelination and EAE [11,13-15]. In primary human OPCs, M_3R signaling delays differentiation *in vitro* and reduces myelin production following into hypomyelinated *shiverer* mice [12]. OPCs have been shown to express numerous other $G\alpha_q$-coupled receptors including endothelin receptors $ET_{A/B}$ (ENDRB) [16], purinergic P2Y [17], histamine H1 [18], metabotropic glutamate receptors 3 (mGluR3) and 5 (mGluR5) [19], 5HT serotonin receptor [20], sphingosine-1-phosphate receptor (S1PR) [21], calcium-sensing receptor (CaSR) [22], and adenosine receptor 2B [23]. While the precise function of these receptors remain unclear, previous reports suggest that activation of at least some of these receptors can paradoxically promote OPC differentiation. For example, *in vitro* ET receptor agonists increase OPC migration and block proliferation [16], stimulate MBP expression via ET_A [24], and via ET_B promoted remyelination in cerebellar slice culture [25]. Likewise, conditional deletion of S1PR causes increased OPC proliferation and reduced oligodendrocyte differentiation [26], while CaSR null mice exhibit reduced MBP expression during development [22]. The key signaling components downstream of

muscarinic receptor activation that act to delay differentiation and distinguish M1/3 from other $G\alpha_q$-receptors have not yet been established.

Following activation of G_qR coupled signaling and calcium release, the ER-calcium sensing STIM proteins oligomerize and complex with ORAI channel proteins located in the plasma membrane. These calcium release activated channels (CRAC) mediate store operated calcium entry (SOCE) that replenish depleted ER-stores through sarcoplasmic/endoplasmic reticulum ATPase (SERCA) pumps [27]. Successive activation of ER-calcium release and CRAC channel influx events result in characteristic oscillatory calcium transients [28]. Intriguingly, the frequency encoding of oscillatory calcium signaling is associated with cell-type specific activation of distinct downstream signaling and gene expression [29,30]. In rodent OPCs, *in vitro* application of a pharmacological SOCE antagonist limits PDGF-dependent proliferation [31]. However, the mechanisms of action of these drugs are complex with additional actions on IP_3 receptors, gap junction permeability, and transient receptor potential channels. Furthermore, while ligand-induced calcium oscillations have been observed in OL lineage cells [19,32,33], a specific role of calcium oscillations has not been determined.

In this study, we hypothesized that the specific oscillatory signature of ligand activated G_qR calcium responses may be responsible for the regulation of hOPC differentiation. To this end, we identified several G_q-coupled receptors expressed by hOPCs and characterized the calcium response following application of receptor subtype-specific ligands. Only activation of muscarinic acetylcholine $M_{1/3}R$ or metabotropic type 5 glutamate receptors ($mGluR_5$) resulted in oscillatory transients in the majority of OPCs that persisted for several minutes following application of the ligand. Intriguingly, these ligands also reduced hOPC differentiation. We demonstrate that SOCE downstream of $M_{1/3}R$ ligand activation is dependent on ER calcium sensors STIM1/2. More specifically, we found that both STIM proteins contribute to the magnitude of SOCE in OPCs and that STIM2 in addition regulates the oscillatory frequency of $M_{1/3}R$-induced calcium responses. Importantly, knockdown of STIM2 resulted in reduced OL differentiation and prevented the anti-differentiative effects of MR-signaling in hOPCs. Lastly, using optogenetic induction of CRAC-mediated calcium influx, we demonstrate that induction of SOCE induction was sufficient to inhibit hOPC differentiation in the absence of G_qR signaling and that modulation of OPC proliferation and differentiation was highly dependent on SOCE frequency.

MATERIALS AND METHODS

Human CD140a/PDGFαR cell preparation and culture with $G\alpha_q$-agonists

Fetal brain tissue samples, between 17 and 22 weeks of gestational age, were obtained from Advanced Bioscience Resources (Alameda, CA) with informed consent obtained from all donors. All research was performed in accordance with relevant guidelines/regulations. Following review by the University at Buffalo Research Subjects Institutional Review Board the tissue acquisition and research was not deemed to involve human subjects as defined under HHS regulations 45 CFR 46, 102 (f). Forebrain samples were minced and dissociated using papain and DNase as previously described [34]. Magnetic sorting of CD140a/PDGFαR positive cells was performed as described [35].

Plasmid construction, lentiviral generation, and titration

EF1α:GCaMP6s was described previously [12]. EF1α:jRCaMP1a was cloned as follows. pGP-CMV-NES-jRCaMP1a was obtained from AddGene (#61562) [36]. The nuclear export signal (NES) and jRCaMP1a coding region was PCR amplified: SpeI, forward–5'-AAAACTAGTGAACCGTCAGATCCGCTAG-3';PspXI (Thermo Fisher Scientific), reverse, 5'-AAAGCTCGAGCTCTACAAATGTGGTATGGCTG-3' (Thermo Fisher Scientific). PCR products were purified (Monarch PCR Cleanup Kit (NEB, #T1030S)) and restriction digested with unique 5' SpeI and 3' PspXI sites, and purified again. NES-jRCaMP1a digested PCR fragments were then ligated into lentiviral pTRIP-EF1α vector (a gift of Abdel Benraiss, University of Rochester)[37]. The plasmid pLenti-EF1α-OptoSTIM was a gift from Taeyoon Kyung (KAIST, DAEJEON, Republic of Korea) [38]. Lentiviruses were generated as described [39] and titration of EF1α:GCaMP6s and EF1α:OptoSTIM was performed as previously described [40]. Optimized multiplicity of infection (MOI) in hOPCs was determined for EF1α:GCaMP6s and EF1α:jRCaMP1a by infecting hOPCs and quantifying proportion of responsive cells following administration of 25µM Oxo-M. Optimal MOI for EF1α:OptoSTIM lentivirus was determined through analysis of optimal GFP expression in infected hOPCs.

Calcium imaging using LV EF1a:GCaMP6s

Calcium imaging was performed as described previously [12]. Briefly, GCaMP6s infected hOPCs were seeded at 4–5 x 10^4 cells/mL and imaged 24 hours after seeding. Bright field and fluorescence images were acquired (10x; Olympus IX51 microscope with a Exfo X-Cite or Xylis illumination and Hamamatsu ORCA-FLASHv4 camera) using µManager [41]. All drugs were reconstituted and aliquoted within 1-2 weeks and thawed immediately prior to use. Region of interest (ROI) generation and image processing was performed using ImageJ, and analysis of calcium transients was performed in R as described [12]. Unless otherwise stated, a linear model was used for one-way ANOVA using drug dose as a covariate, as well as human sample to consider individual sample variability. Non-linear regression was

performed using GraphPad Prism (8.0e) using a variable slope-four parameter logistic equation to model and calculate EC_{50} for each drug. For STIM KD experiments, GCaMP6s cells were transfected with STIM siRNA and imaged 24-48h post transfection.

Assessment of store-operated calcium entry

For direct assessment of SOCE, hOPCs were infected with LV-GCaMP6s (1 MOI) and 5 x 10^4 cells/mL were seeding in 48-well plates and imaged the following day. To remove extracellular calcium, 15 minutes prior to imaging media was replaced with HBSS without phenol red, calcium, and magnesium (Corning, #21-022) (HBSS-). For all conditions, fields were imaged with a 5 second interval for at least 15 minutes (488nm excitation, 400ms exposure). Addition of Thapsigargin (Tg) or Oxo-M with or without SOCC antagonists occurred at ~2 minutes after the start of imaging. Calcium (final concentration: [500µM]) was re-introduced 10-15 minutes following addition of Tg or Oxo-M. Final concentrations of compounds were Tg [10µM] or Oxo-M [25µM], and 2-APB [50µM] or MRS-1845 [10µM] (final DMSO concentration did not exceed 0.15%, which did not influence $[Ca^{2+}]_i$). For quantification of SOCE, per cell calcium response curves were normalized to baseline fluorescence (F_0, average 5-10 frames) prior to addition of Oxo-M or Tg. Normalized traces were loess fitted to identify responsive cells with ≥ 35% increase in GCaMP6s fluorescence to initial Oxo-M or Tg ER-store depletion. As described in [42], area under the curve measurements of responsive cells was analyzed for store depletion (1st peak) and SOCE (2nd peak), and statistical significance was tested on AUC of SOCE normalized to that of ER-Depletion using one-way ANOVA.

siRNA transfection

hOPCs were seeded at 5 x 10^4 cells/mL and Lipofectamine RNAi max (Invitrogen, #13778-150) was used to transfect cells according to the manufacturer's protocol with minor alterations. Briefly, stealth RNAi negative control duplex medium GC content (Invitrogen, #12935300) or three combined stealth RNAis against STIM1 (Invitrogen, ID#'s: HSS110308, HSS110309, HSS186144) and/or STIM2 (Invitrogen, ID#'s: HSS183972, HSS183973, HSS183974) were pooled and used for transfection. Stealth RNAi (100 nM total RNAi per well) was used to transfect hOPCs per each condition with 1.5% v/v Lipofectamine. For calcium imaging, cells were plated in 48-well plates and imaged 24 hours post-transfection. In differentiation experiments, mitogen containing media was removed 24 hours post-transfection (experimental day 0) and replaced with media without mitogens. Oxotremorine [25µM] was added on experimental day 0 upon removal of growth factors and on experimental day 2 during a half media change. hOPCs were fixed on experimental day 3-4 following live staining with mouse x O4 Hybridoma primary antibody [1:25]. Immuno-cytochemical analysis was performed as described previously [34]. For analysis of STIM expression, cells were plated at 5 x 10^4 cells/mL 6-well plates and

transfected after 24 hours. RNA was extracted 24-48 hours post-transfection for cDNA synthesis and quantitative RT-PCR analysis.

Quantitative RT-PCR analyses

Total RNA was extracted (Omega Biotek) and cDNA was synthesized using SuperScript III reverse transcriptase (Invitrogen, Carlsbad, CA). Human-specific primers for SYBR green-based PCR were designed (**Table 1**). Samples were run in triplicate and gene expression calculated by $\Delta\Delta C_t$ method using GAPDH as a reference. Statistical significance was tested on $\log_2$-transformed data normalized to control using a one-sample t-test assuming equal SD and compared to a hypothetical value of 100 (GraphPad Prism 8.0e).

Assessment of long-term OptoSTIM-induced SOCE

For all long-term experiments, hOPCs were seeded at a density of 2.5-3.0 x 10^5 cells/mL into poly-ornithine and laminin coated ibidi tissue culture treated µ-slide VI 0.4 (iBIDI, #80606) in mitogen containing Livelight ND media to reduce phototoxicity [43]. Cells were then imaged in an on-stage ibidi environmentally controlled chamber to maintain 37ºC, 5.0% CO2, and 60% humidity for the duration of each imaging experiment. In long-term calcium imaging experiments, hOPCs were infected with jRCaMP1a (1 MOI) and OptoSTIM (1 MOI) lentiviruses. Two fields per each of 3 µ-slide channels were then imaged at 10x with 594 nm excitation every 20 seconds for 3 hours to measure jRCaMP1a fluorescence calcium responses. After a 30-minute no-stimulation period and for the remainder of imaging, hOPCs were stimulated with 488 nm excitation (every 5 or 30 minutes with 330 and 2000 ms illumination times respectively) to induce SOCE calcium responses. A custom beanshell script was designed and implemented to facilitate multi-channel and multi-position imaging and provide an interface between the motorized stage, fluorescent shutter (Prior), and µManager software. The complete imaging script is available upon request. Analysis of OptoSTIM-induced calcium responses was conducted by implementing the automated tracking plugin TrackMate in ImageJ [44]. Mean fluorescence intensity data within the region of interest for all cells tracked across all frames was exported and subsequently analyzed in R. Briefly, a baseline curve was generated by fitting minima points under each calcium trace using the “spc-Rubberband" function (*hyperSpec* package). Traces were first normalized by division of the baseline curve and loess fitted to identify responsive cells with ≥ 12.5% increase in jRCaMP1a fluorescence within 2 minutes following the first OptoSTIM 488nm pulse. For quantification of AUC, each tracked cell’s mean jRCaMP1a fluorescence values per each time-point were normalized by subtraction of the baseline curve and AUC was calculated for the duration of the stimulation period. Calcium traces are presented as fold change in jRCaMP1a fluorescence from baseline, averaged across all cells per each time-point with SEM calculated. In differentiation and proliferation experiments, OptoSTIM infected

hOPCs (1 MOI) were seeded into µ-slides and bright field imaged for 2–3 days. Following a 10-12 hour baseline period, OptoSTIM activation was initiated with 488nm stimulation at different frequencies (every 5 or 30m with 330 or 2000ms illumination times respectively) for the remainder of imaging. After imaging, cells were immunostained for O4 and the number of $O4^+$ and GFP^+ cells were counted and analyzed. Repeated measures (RM) one-way ANOVA was employed with Tukey or Dunnett's post-hoc test for quantification of the proportion of $O4^+$ to GFP^+ cells and quantification of morphological branching respectively. In proliferation experiments, cell density was counted at the onset of blue light stimulation and mitotic events were identified and counted throughout the stimulation period. RM one-way ANOVA with Tukey's post-hoc test was implemented to quantify significance in proliferative events normalized to initial densities for each condition.

RESULTS

$G\alpha_q$-receptor activation induces ER-Ca^{2+} responses and SOCE in hOPC.

We hypothesized that $G\alpha_q$-coupled receptors would exert distinct effects on intracellular calcium responses in hOPCs and that these responses would correlate with their functional effects. Using RNA-seq of human primary PDGFRα-isolated OPCs, we determined that hOPCs expressed a diverse set of 122 GPCRs including 14 GPCRs that couple via $G\alpha_q$ proteins (GPCRs "GO:0004930" and PLC activating $G\alpha_q$-coupled "GO:0007200", respectively). To determine the nature of $G\alpha_q$-mediated calcium responses in hOPCs, we exposed primary hOPCs to selective ligands at 10-fold the reported EC_{50} and measured calcium responses following viral-mediated expression of the intracellular calcium reporter GCaMP6s (**Fig 1** and **Table 2**). Almost all ligands induced small calcium elevations in a small subset of the hOPC population (1-30%). In contrast, activation of $M_{1/3}R$ and $mGluR_5$ receptors by Oxo-M and CHPG, respectively, elicited robust responses in more than 50% of hOPCs (n = 3 human samples). Both agonists induced a dose-dependent increase in the proportion of responding cells (**Fig 1A-B**). The extent of calcium flux was determined by measuring the area-under-curve (AUC) (mean ± SEM of > 250 cells quantified per each dose, n = 3 human samples). Both agonists induced a clear dose-dependent calcium influx with EC_{50} determined as 2.2 µM and 1.3 mM for Oxo-M and CHPG respectively (**Fig 1C-D**).

The calcium responses to $G\alpha_q$-specific agonists were further classified into monotonic and oscillatory responses (**Table 2**). Intriguingly, of those ligands which resulted in calcium transients in <30% of cells, we often observed that the majority of responses were monotonic and typically short-lived returning to baseline within 3 mins following agonist application. In contrast, agonists for $M_{1/3}R$ and $mGluR_5$ receptors resulted in prolonged oscillatory calcium transients which persisted for over 6 minutes (6.1 ± 0.8 and 6.7 ± 0.1 mins, for Oxo-M and CHPG respectively; mean ± SEM). As such, the calcium responses following activation of $G\alpha_q$-coupled receptors were distinguishable from one another. The similarity of prolonged oscillations in the calcium response following $mGluR_5$ agonist treatment to $M_{1/3}R$ suggested that a common downstream signaling pathway may be engaged compared to other ligands.

As $M_{1/3}R$ activation leads to a profound blockade of hOPC differentiation [12], we hypothesized that the prolonged oscillatory calcium response may underlie this effect and that $mGluR_5$ activation would therefore lead to a similar inhibition of differentiation. In addition, we predicted that EDNRB activation, which instead elicits a minimal and transient calcium response, would not influence hOPC differentiation. To test this hypothesis, we treated hOPCs with ET-1 or CHPG in the absence of mitogens and determined the effect on $O4^+$ oligodendrocyte (OL) differentiation after 3-4 days (**Fig 1-1**). 150 nM and 1.5 µM ET-1 did not influence the proportion of $O4^+$ OLs (RM One-way ANOVA, p=0.64, n = 2 individual human samples). Furthermore, ET-1 did not alter the generation of complex branched $O4^+$ oligodendrocytes

(p=0.59). In contrast, treatment with the $mGluR_5$ agonist CHPG [1.3mM] significantly attenuated $O4^+$ oligodendrocyte differentiation from 42 ± 4% to 32 ± 5% (**Fig 1-1;** RM One-way ANOVA with Tukey's post-hoc test, p=0.0097). Furthermore, CHPG treatment significantly reduced complex branch formation in differentiated $O4^+$ immature oligodendrocytes from 27 ± 4% to 18 ± 5% (p=0.0044) suggesting blockade of oligodendrocyte maturation. These data suggest that distinct patterns of calcium signaling occur following $G\alpha_q$-receptor activation and that oscillatory calcium release may act to block hOPC differentiation and maturation.

SOCE is activated following $M_{1/3}R$ agonist stimulation.

As oscillatory calcium responses are sustained by store-operated calcium entry (SOCE) through the activation of calcium release activated channels (CRAC) (for review see [27], we hypothesized that CRAC channels were activated following $M_{1/3}R$ and $mGluR_5$ $G\alpha_q$-receptor activation and store depletion in hOPCs. Calcium responses in hOPCs were measured following infection with lentivirus encoding calcium reporter GCaMP6s [12]. To investigate whether SOCE occurs following ER Ca^{2+} depletion in hOPCs, we treated cells in the absence of extracellular Ca^{2+} with thapsigargin, a sarco-endoplasmic reticulum Ca^{2+}-ATPases inhibitor (SERCA) blocker (Tg) [45] (**Fig 1E**). After the initial peak in calcium due to store depletion, we observed a clear SOCE associate peak following the re-introduction of calcium into the media. Pre-incubation with CRAC channel inhibitors 2-APB [46] or MRS-1845 [47] essentially abolished SOCE in hOPCs (**Fig 1E**). We quantified SOCE as the ratio of Ca^{2+} influx to Ca^{2+} store release (peak 2 AUC: peak 1 AUC ratio) (n = 2-3 individual human samples, ≥ 70 cells per condition). Treatment with 2-APB or MRS-1845 reduced SOCE by 22-fold and 37-fold relative to Tg alone (**Fig 1F;** Tg: 5.6 ± 0.49 SOCE ratio; Tg+2-APB: 0.25 ± 0.05; Tg+MRS: 0.15 ± 0.01).

To test the hypothesis that $M_{1/3}R$ activation leads directly to SOCE, we assessed SOCE following muscarinic agonist treatment. Similar to Tg treatment, Oxo-M induced robust SOCE following calcium reintroduction (**Fig 1E-F;** 5.8 ± 0.49 SOCE ratio, n = 3 human samples, ≥ 96 cells per condition). Likewise, pre-incubation with MRS-1845 or 2-APB similarly resulted in a substantially reduction of SOCE (**Fig 1F;** RM one-way ANOVA with Holm-Sidak's post-hoc test, p<0.01; Oxo-M+2-APB: 0.46 ± 0.05; Oxo-M+MRS: 2.0 ± 0.16). One-way ANOVA revealed no significant differences in the AUC of ER store depletion between all conditions tested (data not shown, p=0.10). Together these results show that robust SOCE occurs following $G\alpha_q$ induced signaling in hOPCs.

STIM1/2 expression is necessary for muscarinic receptor induced SOCE.

The primary CRAC channel mediating calcium influx in mammalian cells is a channel pore comprised of ORAI channel forming and STIM calcium sensor proteins [27]. RNA-seq analyses revealed expression of both calcium sensors STIM1 and STIM2 mRNA in both mOPCs and hOPCs (mOPCs:

STIM1=13.9 ± 1.4 and STIM2: 14.9 ± 0.7; hOPCs: STIM1=8.69 ± 0.004 and STIM2=30.0 ± 0.56; FPKM ± SEM, n=2). We hypothesized that the calcium sensors STIM1 and STIM2 would be directly involved in regulating calcium influx through CRAC channels following $G\alpha_q$-receptor activation in hOPCs. To test this hypothesis, we used siRNA targeting STIM1 and or STIM2 (STIM KD) coupled with calcium imaging. We observed a 70-85% decrease in mRNA expression of STIM1 (**Fig 2A;** one sample t-test $p<0.0001$) and STIM2 (**Fig 2B;** STIM2 & STIM1/2: $p<0.0001$) following STIM KD in hOPCs. To directly assess the role of STIM proteins in muscarinic receptor-induced SOCE, we assessed calcium influx following extracellular calcium removal and re-addition in the context of STIM1/2 KD and Oxo-M treatment. As shown above, we identified robust SOCE downstream Oxo-M stimulation which was effectively blocked by CRAC antagonist 2-APB. Furthermore, SOCE was substantially attenuated by knockdown of either STIM1 or STIM2 (**Fig 2C-E**) (n=4 human samples, RM one-way ANOVA, Tukey's post-hoc test, $p=0.0002$). Interestingly, the combined KD of both STIM1/2 did not further reduce SOCE suggesting that both sensors are required for muscarinic-induced SOCE and that each STIM protein is a vital component of the endogenous hOPC CRAC apparatus**.** We next sought to investigate the net effects of STIM KD on endogenous hOPC $[Ca^{2+}]_i$ oscillations in the presence of extracellular calcium. The loss of either STIM1 or STIM2 significantly attenuated the overall magnitude of the $[Ca^{2+}]_i$ response to Oxo-M (**Fig 2F**; one-way ANOVA, $p<0.0001$, n=4 human samples). In addition, STIM2 KD resulted in a significant reduction in the frequency of $[Ca^{2+}]$ oscillations (**Fig 2G**; Tukey's post-hoc test, STIM2: $p= 0.002$; STIM1/2: $p=0.0323$) while STIM1 KD had no effect (STIM1: $p = 0.7236$). In summary, these results demonstrate that STIM1 and STIM2 are directly involved in modulating $[Ca^{2+}]_i$ homeostasis, $G\alpha_q$-induced SOCE as well as Ca^{2+} oscillation frequency and magnitude in hOPCs.

STIM2 is required for human oligodendrocyte progenitor differentiation.

To determine whether STIM-dependent calcium oscillations may directly contribute to muscarinic $M_{1/3}R$-mediated inhibition of hOPC differentiation, we assessed the effects of STIM1/2 ablation on hOPC differentiation *in vitro* (**Fig 3A**). While STIM1 siRNA had no effect on hOPC differentiation ($p = 0.42$), STIM2 KD caused a significant reduction in $O4^+$ OL differentiation (RM three-way ANOVA, STIM1 main effect $F(1,3) = 28.64$, $p = 0.013$, n=4 human samples). As shown previously [15], Oxo-M treatment significantly blocked differentiation into $O4^+$ immature OLs (Oxo-M main effect $F(1,3)=14.31$, $p=0.032$). Interestingly, while both control and STIM1 KD hOPCs showed reduced differentiation in response to Oxo-M (**Fig 3B;** Holm-Sidak post-hoc test $p < 0.05$), STIM2 KD abolished the anti-differentiative effects of Oxo-M ($p = 0.49$) suggesting the STIM2 mediated signals were necessary for the effects of Oxo-M on hOPC differentiation. The combination of STIM1 and STIM2 KD also prevented the anti-differentiative effects of Oxo-M on hOPC differentiation. We further examined the effect of STIM1/2 on morphological

maturation by assessing the proportion of $O4^+$ cells with simple or complex process elaboration as described in [34] (**Fig 3-1**). Oxo-M treatment had a significant effect on the proportion of simple $O4^+$ cells (RM three-way ANOVA; $F(1, 3) = 44.76$, $p = 0.0068$) and reduced the proportion of complex $O4^+$ cells following transfect with either control or STIM1 siRNA (**Fig 3-1C**) (Holm-Sidak posttest p=0.0046 and p=0.059, respectively). STIM2 KD selectively reduced the proportion of morphologically mature OLs by >80% ($p = 0.0013$).

As differentiation and OPC proliferation are intimately linked, we examined whether ER calcium sensors STIM1/2 influenced spontaneous hOPC proliferation. We quantified the proportion of dividing $Ki67^+$ OPCs following transfection with STIM1/2 siRNA or control siRNA (**Fig 3C**). As shown previously [15], Oxo-M had no effect on hOPC proliferation. STIM1 siRNA somewhat reduced hOPC proliferation but did not reach significance (n = 3 human samples; three-way ANOVA, $F(1, 2) = 12.57$, $p = 0.071$) whereas STIM2 KD had no effect ($p > 0.1$). Together, the effects of STIM1 and STIM2 on hOPC differentiation and proliferation were not equivalent. When combined the ablation of both STIM1/2 calcium sensors resulted in a mixed phenotype with reduced differentiation and proliferation. While STIM2 appears to be necessary for later stages of OL differentiation and may be required for the effects of muscarinic agonist-mediated inhibition, STIM1 may positively regulate OPC proliferation.

Optogenetically-induced SOCE blocks hOPC differentiation and promotes proliferation.

Our previous results suggest that STIM mediated SOCE may be required for sustained calcium release following $G\alpha_q$ stimulation and thereby contribute to muscarinic inhibition of differentiation. We therefore sought to test whether oscillatory calcium SOCE directly regulates hOPC development. To this end, we expressed an optogenetically controllable STIM protein in hOPCs to enable blue-light control of SOCE in the absence of $G\alpha_q$-ligand stimulation [38]. Following infection with lentiviral OptoSTIM, hOPCs were transduced with lentiviral jRCaMP1a, a red-shifted calcium indicator, to simultaneously measure intracellular Ca^{2+} while induced SOCE [36]. Following blue light activation of OptoSTIM we observed a consistent and robust oscillatory calcium influx which could be sustained for several hours in a frequency-specific manner (**Fig 4A-B**). We selected a higher 3.33 Hz frequency to mimic rapid muscarinic-receptor type SOCE and a lower 0.55 Hz that is below the lower threshold associated with frequency-dependent decoding in other cells [29]. Based on jRCaMP1a, oscillatory OptoSTIM-induced SOCE could be maintained for upto 18 hours in hOPCs *in vitro* without loss of signal. We matched the total blue-light exposure between frequencies and found that the total calcium release over the 2.5 h period was matched between groups (**Fig 4C**; RM one-way ANOVA, Tukey's posttest $p = 0.46$). As such, we could assess frequency dependent effects of SOCE while controlling for total calcium flux.

We examined the effect of optogenetically-induced oscillatory SOCE on hOPC proliferation and differentiation (**Fig 5**). Using time lapse microscopy and concurrent intermittent blue-light stimulation to induce SOCE, we assessed the number of mitotic events (**Fig 5A**) that occurred in the presence of both high and low frequency OptoSTIM1-induced SOCE. Induction of high frequency (3.33 mHz) oscillatory calcium entry produced a clear increase in the number of cumulative mitotic events at 24h and 36h post stimulation respectively (**Fig 5B**, quantified in **C**; RM one-way ANOVA with Tukey's post-hoc test, $p = 0.006$, $n = 4$ human samples). After 36 hours of stimulation, high frequency SOCE resulted in a 40% increase rate of cell division relative to unstimulated control hOPCs (3.33 mHz: 25.6 ± 4.9% vs. control: 19.1 ± 4.7%, $p = 0.017$) (**Fig 5C**). In contrast, low frequency SOCE had no effect on proliferation (0.55 mHz; 17.6 ± 5.9%, $p = 0.63$). Next, we investigated the effects of calcium influx on hOPC differentiation after long term OptoSTIM induction (**Fig 5D**). We observed no gross alterations in transduced cell number following blue-light stimulation (**Fig 5E;** RM one-way ANOVA with Tukey's post-hoc test, $p = 0.90$, $n = 4$ human samples). Importantly, induction of high frequency SOCE substantially impaired hOPC differentiation by 50% relative to unstimulated control hOPCs (**Fig 5F**) (3.33 mHz: 7.5 ± 1.7% $O4^+/GFP^+$ cells vs. control: 16.6 ± 3.4, $p = 0.024$). The lower frequency SOCE exhibited a small and nonsignificant effect on differentiation (0.55 mHz: 12.83 ± 3.3%). Moreover, we identified a significant reduction in complex $O4^+$ cells following 3.33 mHz stimulation compared to control cells (**Fig 5G**). Collectively these results indicate that sustained high frequency oscillatory SOCE was sufficient to both block hOPC differentiation and augment hOPC proliferation.

DISCUSSION

In the present study, we demonstrate that a subset of $G\alpha_q$ receptors expressed by human primary OPCs, including $M_{1/3}R$ and mGluR5, induced prolonged oscillatory calcium signaling and that the ability to induce oscillatory calcium signaling correlated with their capacity to block differentiation. We found that a common mechanism downstream of oscillatory $G\alpha_q$ signaling was the activation of store operated calcium entry (SOCE). Inhibition of SOCE either pharmacologically or via knockdown of ER-localized calcium sensors STIM1/2 reduced the extent and amount of calcium signaling induced by $G\alpha_q$ ligand application. STIM2 ablation selectively reduced calcium oscillation frequency and spontaneous OL differentiation *in vitro* and, unlike control OPCs, treatment with muscarinic ligand did not further reduce differentiation following STIM2 knockdown. This suggested a functional linkage between muscarinic receptor signaling and SOCE. Using an optogenetic approach to selectively activate SOCE in OPCs, we found that SOCE was sufficient to modulate OL differentiation in the absence of $G\alpha_q$ dependent signaling suggesting that calcium release is a key facet in the muscarinic pathway that impairs OL differentiation and remyelination. Furthermore, the frequency of SOCE rather overall amount of calcium release was found to be vital in mediating the effect of calcium entry on differentiation and proliferation. This suggests that the calcium pathway includes frequency-dependent 'decoders' which regulate OL differentiation and that modulation of calcium frequency might represent an important mechanism by which diverse signals are integrated by parenchymal OPCs.

In drug development, G-protein coupled receptors (GPCRs) are attractive candidates for therapeutic intervention and recently many small molecules that target GPCRs have been identified that modulate OPC function and OL differentiation to promote myelin repair [48]. For example, GPR17 which largely couples via $G\alpha_{i/o}$ was found to negatively regulate OPC differentiation while knockout was observed to promote remyelination [49]. Muscarinic receptor antagonists have displayed a remarkable capacity to improve OL differentiation and remyelination in various animal models. Using genetic approaches, the effects of these drugs have been localized to M_1R and M_3R. Both of these receptors represent canonical $G\alpha_q$-coupled receptors. Indeed, when $G\alpha$ coupling was systematically analyzed across different subunit, M_3R displayed exquisite selectivity for rapid activation for $G\alpha_q/G\alpha_{11}$ coupling [50]. In this study, we focused on $G\alpha_q$-coupled receptors to determine if a shared characteristic of $G\alpha_q$ receptors could be used to predict their ability to prevent efficient OL differentiation and thereby impair remyelination. We analyzed RNA-seq analysis of primary hOPC to identity those $G\alpha_q$-coupled receptors expressed at the mRNA level and hypothesized that receptor-specific ligand activation would produce canonical oscillatory calcium signaling and block hOPC differentiation. Surprisingly, only a small subset of pharmacological $G\alpha_q$ ligands were capable of inducing prolonged calcium oscillation in hOPCs.

Intriguingly, this correlated with the ability of ligands to effectively block OL differentiation. CHPG which activates $mGluR_5$ (GRM5) in a highly selective manner was the only other ligand capable of inducing calcium oscillations in the majority of responding cells. GRM5 couples primarily via $G\alpha_q$ but does not have appreciable activity at $G\alpha_i$. In a similar manner to M_3R, $mGluR_5$ mRNA was relatively highly expressed in rodent OPCs and down-regulated following differentiation [19]. Herein, we found that treatment with CHPG resulted in a dose-dependent blockade of hOPC differentiation.

In contrast, the other $G\alpha_q$ couple receptors that elicited calcium responses in OPCs induced calcium release that was either considerably shorter in duration and/or were largely monotonic in nature. These differences could be due to differences in overall level of expression and/or differences in receptor coupling. From a large-scale screen of G-protein coupling [51], we observed that many of these receptors were promiscuously coupled with other $G\alpha$ subunits. For example, S1PR1 was observed as primarily coupled via $G\alpha_i$ and $G\alpha_o$ with little evidence of $G\alpha_q$ coupling. This difference corresponded with the observed function difference following activation of S1PR1 which results in OL differentiation from human OPCs [52]. Furthermore, ENDRB, F2R and P2RY1 each show promiscuously with multiple $G\alpha$ proteins activated. Together this suggests that selectively in coupling may influence the net influence on downstream signaling and the nature of the resultant calcium response. As the coupling of GPCRs to specific $G\alpha$ proteins are not absolute and in many cases is promiscuous, we anticipate that biased ligands or antagonists capable of promoting or blocking coupling along specific pathways may represent optimal approaches to promote OPC differentiation.

The mechanisms which shape the calcium-response following ligand application are complex and likely dependent on multiple interacting proteins. Among these, $G\alpha$ subunits form specific complexes with their cognate $G\beta\gamma$ proteins which possess their own signaling capability and modulate the signaling of $G\alpha$ subunits they interact with [53]. Among these, specific isoforms of PI3K and adenylate cyclase, voltage-operated calcium channels (VOCC) and inwardly rectifying K^+ channel can be regulated by $G\beta\gamma$. Activation of PI3K/Akt [54], adenylate cyclase [55], and VOCC [56] are associated with promotion of OPC differentiation suggesting that $G\beta\gamma$ activation may counteract oscillatory calcium signaling. For muscarinic receptor signaling, in rat pituitary cells $G_{\beta3}$ is necessary for the carbachol-mediated calcium current [57], while in a rat leukemia cell line $G_{\beta1}$ and $G_{\beta4}$ were more important in the regulation of this current [58]. In primary hOPCs, $G_{\beta4}$ ablation did not influence calcium signaling following oxo-M treatment [59]. Redundancy with $G_{\beta1}$ and $G_{\beta2}$ is possible as these subunits are expressed at substantially higher levels in human, rat, and mouse OPCs.

In addition to the $G_{\beta\gamma}$ subunit specific regulation, receptor-specific activation of regulators of G-protein signaling (RGS) proteins provide specificity for G-protein coupling and modulate the kinetics of

second messenger activation [60]. RGS proteins promote termination of GPCR signaling via GTPase activation and in the absence of ligand prevent GPCR signaling. Following ligand activation, RGS proteins exhibit a cyclical pattern of association with PIP_3, Ca^{2+}/CaM, and finally after Ca^{2+} levels return to baseline reassociation with the GPCR complex. This allows a second cycle to start and initiate another calcium spike. The kinetics of these steps, especially the slow dissociation of RGS protein from Ca^{2+}/CaM, contributes to the resultant frequency of calcium oscillations [61]. While the role of specific RGS proteins in the OPC and oligodendrocyte lineage is poorly understood, several RGS proteins are expressed in OPCs [62]. Among these RGS4 has been shown to potently influence negatively influence muscarinic receptor signaling in insulinoma cells [63]. Also noteworthy, the R7 family of RGS proteins (RGS6/7/9/11) form heterodimers with G-protein β subunit Gβ5 (GNB5) which similarly attenuate M_3R-dependent Ca^{2+} signaling [64].

Once activated SOCE is associated with many cellular functions in neural progenitors such as proliferation [65] and differentiation [66,67]. In OPCs, SOCE can modulate PDGF-AA induced OPC proliferation [31]. However, given the known role of PI3K/Akt signaling downstream of PDGF receptor, SOCE is unlikely to be a critical component of PDGF signaling. Likewise, the cellular role of calcium oscillations in OPC soma is not yet known. Our data indicate that SOCE along is sufficient to modulate both OPC proliferation and differentiation and that oscillatory SOCE only occurs following application of specific G_q-receptor agonists. The specificity of G_q-receptor mediated signaling is consistent with previous results which have shown that while endothelin (ET) agonist treatment induces a monotonic calcium response [24] while metabotropic glutamate receptor agonists induce OPC oscillations [19]. SOCE itself is dependent on the association of CRAC subunit comprising STIM ER-calcium sensors and ORAI channel subunits. While both STIM1/2 contributed to the magnitude of SOCE in hOPCs, we found that only STIM2 knockdown reduced spontaneous OL differentiation. The ER-calcium sensors STIM1/2 physically and functionally interact with one another to regulate SOCE [68]. The relative abundance of STIM1 and STIM2 vary greatly between tissues and individual cell types. In human OPCs, STIM2 is more than 3-fold more abundant than STIM1 mRNA but both genes are relatively highly expressed (>10 FPKM). In contrast, both STIM1 and STIM2 are expressed at equivalent levels in mouse OPCs [62]. As the differences in the relative expression of STIM1/2 influences the resultant properties of SOCE in response to store depletion see [69 for review], the differences in STIM1:STIM2 ratio in mouse and human may therefore underlie some of the species-specific functional differences in OPC behavior [70]. Both STIM1 and STIM2 have been shown to contribute to oscillatory SOCE in a context dependent manner [71,72]. Our data support a specific role of STIM2 in the regulation of OPC calcium oscillation and also suggest that expression of STIM2 is required for muscarinic receptor induced differentiation blockade in hOPCs. Together with the direct regulation of OPC differentiation via optogenetically-gated SOCE, these data suggest that SOCE

mediated via STIM activation will likely play an important role in mediating the negative effects of G_q-coupled receptors capable of blocking oligodendrocyte differentiation in health and disease.

REFERENCES

1 Franklin, R. J. M. & Ffrench-Constant, C. Regenerating CNS myelin - from mechanisms to experimental medicines. *Nature reviews. Neuroscience* **18**, 753-769, doi:10.1038/nrn.2017.136 (2017).

2 Faissner, S., Plemel, J. R., Gold, R. & Yong, V. W. Progressive multiple sclerosis: from pathophysiology to therapeutic strategies. *Nat Rev Drug Discov* **18**, 905-922, doi:10.1038/s41573-019-0035-2 (2019).

3 Kuhlmann, T. *et al.* Differentiation block of oligodendroglial progenitor cells as a cause for remyelination failure in chronic multiple sclerosis. *Brain : a journal of neurology* **131**, 1749-1758, doi:10.1093/brain/awn096 (2008).

4 Wolswijk, G. Chronic stage multiple sclerosis lesions contain a relatively quiescent population of oligodendrocyte precursor cells. *J Neurosci* **18**, 601-609 (1998).

5 Thornton, M. A. & Hughes, E. G. Neuron-oligodendroglia interactions: Activity-dependent regulation of cellular signaling. *Neuroscience letters* **727**, 134916, doi:10.1016/j.neulet.2020.134916 (2020).

6 Ortiz, F. C. *et al.* Neuronal activity in vivo enhances functional myelin repair. *JCI Insight* **5**, doi:10.1172/jci.insight.123434 (2019).

7 Gautier, H. O. *et al.* Neuronal activity regulates remyelination via glutamate signalling to oligodendrocyte progenitors. *Nat Commun* **6**, 8518, doi:10.1038/ncomms9518 (2015).

8 Bernstein, M., Lyons, S. A., Moller, T. & Kettenmann, H. Receptor-mediated calcium signalling in glial cells from mouse corpus callosum slices. *Journal of neuroscience research* **46**, 152-163, doi:10.1002/(SICI)1097-4547(19961015)46:2<152::AID-JNR3>3.0.CO;2-G (1996).

9 Paez, P. M. & Lyons, D. A. Calcium Signaling in the Oligodendrocyte Lineage: Regulators and Consequences. *Annual review of neuroscience* **43**, 163-186, doi:10.1146/annurev-neuro-100719-093305 (2020).

10 Berridge, M. J. & Irvine, R. F. Inositol phosphates and cell signalling. *Nature* **341**, 197-205, doi:10.1038/341197a0 (1989).

11 Mei, F. *et al.* Accelerated remyelination during inflammatory demyelination prevents axonal loss and improves functional recovery. *Elife* **5**, e18246, doi:10.7554/eLife.18246 (2016).

12 Welliver, R. R. *et al.* Muscarinic Receptor M3R Signaling Prevents Efficient Remyelination by Human and Mouse Oligodendrocyte Progenitor Cells. *J Neurosci* **38**, 6921-6932, doi:10.1523/JNEUROSCI.1862-17.2018 (2018).

13 Mei, F. *et al.* Micropillar arrays as a high-throughput screening platform for therapeutics in multiple sclerosis. *Nature medicine* **20**, 954-960, doi:10.1038/nm.3618 (2014).

14 Deshmukh, V. A. *et al.* A regenerative approach to the treatment of multiple sclerosis. *Nature* **502**, 327-332, doi:10.1038/nature12647 (2013).

15 Abiraman, K. *et al.* Anti-muscarinic adjunct therapy accelerates functional human oligodendrocyte repair. *J Neurosci* **35**, 3676-3688, doi:10.1523/JNEUROSCI.3510-14.2015 (2015).

16 Gadea, A., Aguirre, A., Haydar, T. F. & Gallo, V. Endothelin-1 regulates oligodendrocyte development. *J Neurosci* **29**, 10047-10062, doi:10.1523/JNEUROSCI.0822-09.2009 (2009).

17 Agresti, C. *et al.* ATP regulates oligodendrocyte progenitor migration, proliferation, and differentiation: involvement of metabotropic P2 receptors. *Brain Res Brain Res Rev* **48**, 157-165, doi:10.1016/j.brainresrev.2004.12.005 (2005).

18 Takeda, M., Nelson, D. J. & Soliven, B. Calcium signaling in cultured rat oligodendrocytes. *Glia* **14**, 225-236, doi:10.1002/glia.440140308 (1995).

19 Luyt, K., Varadi, A., Durant, C. F. & Molnar, E. Oligodendroglial metabotropic glutamate receptors are developmentally regulated and involved in the prevention of apoptosis. *J Neurochem* **99**, 641-656, doi:10.1111/j.1471-4159.2006.04103.x (2006).

20 Fan, L. W. *et al.* Exposure to serotonin adversely affects oligodendrocyte development and myelination in vitro. *J Neurochem* **133**, 532-543, doi:10.1111/jnc.12988 (2015).

21 Jung, C. G. *et al.* Functional consequences of S1P receptor modulation in rat oligodendroglial lineage cells. *Glia* **55**, 1656-1667, doi:10.1002/glia.20576 (2007).

22 Chattopadhyay, N. *et al.* Calcium receptor expression and function in oligodendrocyte commitment and lineage progression: potential impact on reduced myelin basic protein in CaR-null mice. *Journal of neuroscience research* **86**, 2159-2167, doi:10.1002/jnr.21662 (2008).

23 Coppi, E. *et al.* Adenosine A2B receptors inhibit K(+) currents and cell differentiation in cultured oligodendrocyte precursor cells and modulate sphingosine-1-phosphate signaling pathway. *Biochem Pharmacol* **177**, 113956, doi:10.1016/j.bcp.2020.113956 (2020).

24 Jung, K. J. *et al.* The role of endothelin receptor A during myelination of developing oligodendrocytes. *J Korean Med Sci* **26**, 92-99, doi:10.3346/jkms.2011.26.1.92 (2011).

25 Yuen, T. J. *et al.* Identification of endothelin 2 as an inflammatory factor that promotes central nervous system remyelination. *Brain : a journal of neurology* **136**, 1035-1047, doi:10.1093/brain/awt024 (2013).

26 Dukala, D. E. & Soliven, B. S1P1 deletion in oligodendroglial lineage cells: Effect on differentiation and myelination. *Glia* **64**, 570-582, doi:10.1002/glia.22949 (2016).

27 Prakriya, M. & Lewis, R. S. Store-Operated Calcium Channels. *Physiol Rev* **95**, 1383-1436, doi:10.1152/physrev.00020.2014 (2015).

28 Chen, P. J. *et al.* A phase III trial of muparfostat (PI-88) as adjuvant therapy in patients with hepatitis virus related hepatocellular carcinoma (HV-HCC) after resection. *Annals of Oncology* **28**, doi:10.1093/annonc/mdx369.008 (2017).

29 Smedler, E. & Uhlen, P. Frequency decoding of calcium oscillations. *Biochim Biophys Acta* **1840**, 964-969, doi:10.1016/j.bbagen.2013.11.015 (2014).

30 Samanta, K. & Parekh, A. B. Spatial Ca(2+) profiling: decrypting the universal cytosolic Ca(2+) oscillation. *J Physiol* **595**, 3053-3062, doi:10.1113/JP272860 (2017).

31 Paez, P. M. *et al.* Regulation of store-operated and voltage-operated Ca2+ channels in the proliferation and death of oligodendrocyte precursor cells by golli proteins. *ASN Neuro* **1**, doi:10.1042/AN20090003 (2009).

32 Schmidt, C., Ohlemeyer, C., Kettenmann, H., Reutter, W. & Horstkorte, R. Incorporation of N-propanoylneuraminic acid leads to calcium oscillations in oligodendrocytes upon the application of GABA. *Febs Letters* **478**, 276-280, doi:Doi 10.1016/S0014-5793(00)01868-8 (2000).

33 Paez, P. M., Fulton, D., Spreuer, V., Handley, V. & Campagnoni, A. T. Modulation of canonical transient receptor potential channel 1 in the proliferation of oligodendrocyte precursor cells by the golli products of the myelin basic protein gene. *J Neurosci* **31**, 3625-3637, doi:10.1523/JNEUROSCI.4424-10.2011 (2011).

34 Conway, G. D., O'Bara, M. A., Vedia, B. H., Pol, S. U. & Sim, F. J. Histone deacetylase activity is required for human oligodendrocyte progenitor differentiation. *Glia* **60**, 1944-1953, doi:10.1002/glia.22410 (2012).

35 Pol, S. U. *et al.* Sox10-MCS5 enhancer dynamically tracks human oligodendrocyte progenitor fate. *Experimental neurology* **247**, 694-702, doi:10.1016/j.expneurol.2013.03.010 (2013).

36 Dana, H. *et al.* Sensitive red protein calcium indicators for imaging neural activity. *Elife* **5**, doi:10.7554/eLife.12727 (2016).

37 Sevin, C. *et al.* Intracerebral adeno-associated virus-mediated gene transfer in rapidly progressive forms of metachromatic leukodystrophy. *Hum Mol Genet* **15**, 53-64, doi:10.1093/hmg/ddi425 (2006).

38 Kyung, T. *et al.* Optogenetic control of endogenous Ca(2+) channels in vivo. *Nature biotechnology* **33**, 1092-1096, doi:10.1038/nbt.3350 (2015).

39 Wang, J. *et al.* Paired Related Homeobox Protein 1 Regulates Quiescence in Human Oligodendrocyte Progenitors. *Cell reports* **25**, 3435-3450 e3436, doi:10.1016/j.celrep.2018.11.068 (2018).

40 Geraerts, M., Willems, S., Baekelandt, V., Debyser, Z. & Gijsbers, R. Comparison of lentiviral vector titration methods. *BMC biotechnology* **6**, 34, doi:10.1186/1472-6750-6-34 (2006).

41 Edelstein, A., Amodaj, N., Hoover, K., Vale, R. & Stuurman, N. Computer control of microscopes using microManager. *Current protocols in molecular biology* **Chapter 14**, Unit14.20, doi:10.1002/0471142727.mb1420s92 (2010).

42 Davis, F. M. *et al.* Non-stimulated, agonist-stimulated and store-operated Ca2+ influx in MDA-MB-468 breast cancer cells and the effect of EGF-induced EMT on calcium entry. *PLoS One* **7**, e36923, doi:10.1371/journal.pone.0036923 (2012).

43 Stockley, J. H. *et al.* Surpassing light-induced cell damage in vitro with novel cell culture media. *Sci Rep* **7**, 849, doi:10.1038/s41598-017-00829-x (2017).

44 Tinevez, J. Y. *et al.* TrackMate: An open and extensible platform for single-particle tracking. *Methods* **115**, 80-90, doi:10.1016/j.ymeth.2016.09.016 (2017).

45 Treiman, M., Caspersen, C. & Christensen, S. B. A tool coming of age: thapsigargin as an inhibitor of sarco-endoplasmic reticulum Ca(2+)-ATPases. *Trends in pharmacological sciences* **19**, 131-135, doi:10.1016/s0165-6147(98)01184-5 (1998).

46 DeHaven, W. I., Smyth, J. T., Boyles, R. R., Bird, G. S. & Putney, J. W., Jr. Complex actions of 2-aminoethyldiphenyl borate on store-operated calcium entry. *The Journal of biological chemistry* **283**, 19265-19273, doi:10.1074/jbc.M801535200 (2008).

47 Harper, J. L. *et al.* Dihydropyridines as inhibitors of capacitative calcium entry in leukemic HL-60 cells. *Biochem Pharmacol* **65**, 329-338, doi:10.1016/s0006-2952(02)01488-0 (2003).

48 Mogha, A., D'Rozario, M. & Monk, K. R. G Protein-Coupled Receptors in Myelinating Glia. *Trends in pharmacological sciences* **37**, 977-987, doi:10.1016/j.tips.2016.09.002 (2016).

49 Ou, Z. *et al.* Olig2-Targeted G-Protein-Coupled Receptor Gpr17 Regulates Oligodendrocyte Survival in Response to Lysolecithin-Induced Demyelination. *J Neurosci* **36**, 10560-10573, doi:10.1523/JNEUROSCI.0898-16.2016 (2016).

50 Masuho, I. *et al.* Distinct profiles of functional discrimination among G proteins determine the actions of G protein-coupled receptors. *Sci Signal* **8**, ra123, doi:10.1126/scisignal.aab4068 (2015).

51 Inoue, A. *et al.* Illuminating G-Protein-Coupling Selectivity of GPCRs. *Cell* **177**, 1933-1947 e1925, doi:10.1016/j.cell.2019.04.044 (2019).

52 Cui, Q. L., Fang, J., Kennedy, T. E., Almazan, G. & Antel, J. P. Role of p38MAPK in S1P receptor-mediated differentiation of human oligodendrocyte progenitors. *Glia* **62**, 1361-1375, doi:https://doi.org/10.1002/glia.22688 (2014).

53 Khan, S. M. *et al.* The expanding roles of Gbetagamma subunits in G protein-coupled receptor signaling and drug action. *Pharmacological reviews* **65**, 545-577, doi:10.1124/pr.111.005603 (2013).

54 Goebbels, S. *et al.* Elevated phosphatidylinositol 3,4,5-trisphosphate in glia triggers cell-autonomous membrane wrapping and myelination. *J Neurosci* **30**, 8953-8964, doi:10.1523/jneurosci.0219-10.2010 (2010).

55 Raible, D. W. & McMorris, F. A. Induction of oligodendrocyte differentiation by activators of adenylate cyclase. *Journal of neuroscience research* **27**, 43-46, doi:https://doi.org/10.1002/jnr.490270107 (1990).

56 Cheli, V. T. *et al.* Conditional Deletion of the L-Type Calcium Channel Cav1.2 in Oligodendrocyte Progenitor Cells Affects Postnatal Myelination in Mice. *J Neurosci* **36**, 10853-10869, doi:10.1523/JNEUROSCI.1770-16.2016 (2016).

57 Kleuss, C., Scherübl, H., Hescheler, J., Schultz, G. & Wittig, B. Different β-subunits determine G-protein interaction with transmembrane receptors. *Nature* **358**, 424-426, doi:10.1038/358424a0 (1992).

58 Dippel, E., Kalkbrenner, F., Wittig, B. & Schultz, G. A heterotrimeric G protein complex couples the muscarinic m1 receptor to phospholipase C-beta. *Proceedings of the National Academy of Sciences* **93**, 1391-1396, doi:10.1073/pnas.93.4.1391 (1996).

59 Pol, S. U. *et al.* Network-Based Genomic Analysis of Human Oligodendrocyte Progenitor Differentiation. *Stem cell reports* **9**, 710-723, doi:10.1016/j.stemcr.2017.07.007 (2017).

60 Kach, J., Sethakorn, N. & Dulin, N. O. A finer tuning of G-protein signaling through regulated control of RGS proteins. *Am J Physiol Heart Circ Physiol* **303**, H19-35, doi:10.1152/ajpheart.00764.2011 (2012).

61 Luo, X., Popov, S., Bera, A. K., Wilkie, T. M. & Muallem, S. RGS Proteins Provide Biochemical Control of Agonist-Evoked [Ca2+]i Oscillations. *Molecular cell* **7**, 651-660, doi:https://doi.org/10.1016/S1097-2765(01)00211-8 (2001).

62 Zhang, Y. *et al.* An RNA-sequencing transcriptome and splicing database of glia, neurons, and vascular cells of the cerebral cortex. *J Neurosci* **34**, 11929-11947, doi:10.1523/JNEUROSCI.1860-14.2014 (2014).

63 Ruiz de Azua, I. *et al.* RGS4 is a negative regulator of insulin release from pancreatic β-cells in vitro and in vivo. *Proceedings of the National Academy of Sciences* **107**, 7999-8004, doi:10.1073/pnas.1003655107 (2010).

64 Karpinsky-Semper, D., Volmar, C. H., Brothers, S. P. & Slepak, V. Z. Differential effects of the Gβ5-RGS7 complex on muscarinic M3 receptor-induced Ca2+ influx and release. *Mol Pharmacol* **85**, 758-768, doi:10.1124/mol.114.091843 (2014).

65 Domenichini, F. *et al.* Store-Operated Calcium Entries Control Neural Stem Cell Self-Renewal in the Adult Brain Subventricular Zone. *Stem Cells* **36**, 761-774, doi:10.1002/stem.2786 (2018).

66 Forostyak, O. *et al.* Physiology of Ca(2+) signalling in stem cells of different origins and differentiation stages. *Cell Calcium* **59**, 57-66, doi:10.1016/j.ceca.2016.02.001 (2016).

67 Gopurappilly, R., Deb, B. K., Chakraborty, P. & Hasan, G. Stable STIM1 Knockdown in Self-Renewing Human Neural Precursors Promotes Premature Neural Differentiation. *Front Mol Neurosci* **11**, 178, doi:10.3389/fnmol.2018.00178 (2018).

68 López, E., Salido, G. M., Rosado, J. A. & Berna-Erro, A. Unraveling STIM2 function. *J Physiol Biochem* **68**, 619-633, doi:10.1007/s13105-012-0163-1 (2012).

69 Berna-Erro, A., Jardin, I., Salido, G. M. & Rosado, J. A. Role of STIM2 in cell function and physiopathology. *J Physiol* **595**, 3111-3128, doi:10.1113/jp273889 (2017).

70 Dietz, K. C., Polanco, J. J., Pol, S. U. & Sim, F. J. Targeting human oligodendrocyte progenitors for myelin repair. *Experimental neurology* **283**, 489-500, doi:10.1016/j.expneurol.2016.03.017 (2016).

71 Kar, P., Bakowski, D., Di Capite, J., Nelson, C. & Parekh, A. B. Different agonists recruit different stromal interaction molecule proteins to support cytoplasmic Ca2+ oscillations and gene expression. *Proc Natl Acad Sci U S A* **109**, 6969-6974, doi:10.1073/pnas.1201204109 (2012).

72 Thiel, M., Lis, A. & Penner, R. STIM2 drives Ca2+ oscillations through store-operated Ca2+ entry caused by mild store depletion. *J Physiol* **591**, 1433-1445, doi:10.1113/jphysiol.2012.245399 (2013).

73 Harriss, D. R., Marsh, K. A., Birmingham, A. T. & Hill, S. J. Expression of muscarinic M3-receptors coupled to inositol phospholipid hydrolysis in human detrusor cultured smooth muscle cells. *J Urol* **154**, 1241-1245 (1995).

74 Doherty, A. J., Palmer, M. J., Henley, J. M., Collingridge, G. L. & Jane, D. E. (RS)-2-chloro-5-hydroxyphenylglycine (CHPG) activates mGlu5, but no mGlu1, receptors expressed in CHO cells and potentiates NMDA responses in the hippocampus. *Neuropharmacology* **36**, 265-267, doi:10.1016/s0028-3908(97)00001-4 (1997).

75 Pennington, L. D. *et al.* 4-Methoxy-N-[2-(trifluoromethyl)biphenyl-4-ylcarbamoyl]nicotinamide: A Potent and Selective Agonist of S1P1. *ACS Med Chem Lett* **2**, 752-757, doi:10.1021/ml2001399 (2011).

76 Vassallo, R. R., Jr., Kieber-Emmons, T., Cichowski, K. & Brass, L. F. Structure-function relationships in the activation of platelet thrombin receptors by receptor-derived peptides. *The Journal of biological chemistry* **267**, 6081-6085 (1992).

77 Calleri, E. *et al.* Frontal affinity chromatography-mass spectrometry useful for characterization of new ligands for GPR17 receptor. *J Med Chem* **53**, 3489-3501, doi:10.1021/jm901691y (2010).

78 Kawanabe, Y., Okamoto, Y., Enoki, T., Hashimoto, N. & Masaki, T. Ca(2+) channels activated by endothelin-1 in CHO cells expressing endothelin-A or endothelin-B receptors. *American journal of physiology. Cell physiology* **281**, C1676-1685, doi:10.1152/ajpcell.2001.281.5.C1676 (2001).

79 Chhatriwala, M. *et al.* Induction of novel agonist selectivity for the ADP-activated P2Y1 receptor versus the ADP-activated P2Y12 and P2Y13 receptors by conformational constraint of an ADP analog. *The Journal of pharmacology and experimental therapeutics* **311**, 1038-1043, doi:10.1124/jpet.104.068650 (2004).

80 Li, Z., He, Y., Fan, S. & Sun, B. Clemastine rescues behavioral changes and enhances remyelination in the cuprizone mouse model of demyelination. *Neurosci Bull* **31**, 617-625, doi:10.1007/s12264-015-1555-3 (2015).

81 McGuire, J. J., Saifeddine, M., Triggle, C. R., Sun, K. & Hollenberg, M. D. 2-furoyl-LIGRLO-amide: a potent and selective proteinase-activated receptor 2 agonist. *The Journal of pharmacology and experimental therapeutics* **309**, 1124-1131, doi:10.1124/jpet.103.064584 (2004).

82 Tabarean, I. V. Functional pharmacology of H1 histamine receptors expressed in mouse preoptic/anterior hypothalamic neurons. *Br J Pharmacol* **170**, 415-425, doi:10.1111/bph.12286 (2013).

83 Console-Bram, L., Brailoiu, E., Brailoiu, G. C., Sharir, H. & Abood, M. E. Activation of GPR18 by cannabinoid compounds: a tale of biased agonism. *Br J Pharmacol* **171**, 3908-3917, doi:10.1111/bph.12746 (2014).

84 Hinz, S., Lacher, S. K., Seibt, B. F. & Muller, C. E. BAY60-6583 acts as a partial agonist at adenosine A2B receptors. *The Journal of pharmacology and experimental therapeutics* **349**, 427-436, doi:10.1124/jpet.113.210849 (2014).

85 Warren, L. *et al.* Highly efficient reprogramming to pluripotency and directed differentiation of human cells with synthetic modified mRNA. *Cell stem cell* **7**, 618-630, doi:10.1016/j.stem.2010.08.012 (2010).

TABLES

Primer	Sequence 5'-3'
WPRE	Forward: CGCTGCTTTAATGCCTTTGTAT
	Reverse: GGGCCACAACTCCTCATAAA
GAPDH	Forward: GTGAAGGTCGGAGTCAACGG
	Reverse: CCTGGAAGATGGTGATGGGA
STIM1	Forward: CCTCTCTTGACTCGCCATAATC
	Reverse: CTTGGAGTAACGGTTCTGGATATAG
STIM2	Forward: CAACACACACCACACTCCTT
	Reverse: GCCTCTTCCTCCTCTTCATTTC

Table 1: qPCR primers.

Gene Symbol	FPKM (hOPC; mOPCs)	Agonist/ Doses tested	Reported EC_{50}	% Responsive	Maximum amplitude	Duration (min)	% Oscillatory
CHRM3	16.3 ± 2.0; 0.27 ± 0.11	Oxo-M [25 µM]	2.5 µM [73]	67.6 ± 10.0	2.17 ± 0.06	6.1 ± 0.8	63.8 ± 16.2
CHRM1	4.0 ± 0.9; 2.06 ± 0.66						
GRM5	1.2 ± 0.004; 13.23 ± 3.63	CHPG [7.5 mM]	750µM [74]	46.9 ± 9.7	0.87 ± 0.03	6.7 ± 0.1	51.3 ± 5.6
S1PR1	3.1 ± 0.3; 34.32 ± 8.80	TC-G 1006 [350 nM]	35 nM [75]	27.8 ± 2.3	0.6 ± 0.02	2.3 ± 0.2	24.0 ± 14.0
F2R	26.7 ± 0.1; 23.54 ± 3.31	TRAP-6 [8.0 µM]	800 nM [76]	21.2 ± 13.3	1.0 ± 0.10	2.8 ± 0.5	38.9 ± 7.3
GPR17	3.6 ± 1.4; 440.98 ± 42.13	PF9 [400 pM]	36 pM [77]	19.3 ± 0.7	0.6 ± 0.01	2.3 ± 0.3	17 ± 10.3
EDNRB	17.3 ± 01; 292.72 ± 10.54	ET-1 [150 nM]	10 nM [78]	16.8 ± 4.3	1.03 ± 0.09	2.4 ± 0.3	28.8 ± 5.6
P2RY1	1.0 ± 0.2; 4.94 ± 1.46	MRS 2365 [12 nM]	1.2 nM [79]	14.6 ± 8.4	2.9 ± 0.2	9.3 ± 0.9	48.3 ± 0.3
HTR2B	0.8 ± 0.2; 0.12 ± 0.02	5-HT [100 µM]	* 10 µM [80]	13.0 ± 12.4	0.7 ± 0.08	2.1 ± 0.1	14.3 ± 14.3
F2RL1	1.3 ± 0.02; 0.10 ± 0.10	2-FLY [1.0 µM]	2-FLA: 100 nM [81]	8.5 ± 1.3	–	–	–
HRH1	0.4 ± 0.1; 5.01 ± 0.49	2-PED [560 µM]	56 µM [82]	7.4 ± 3.7	–	–	–
GPR18	0.9 ± 0.4; 0.10 ± 0.10	NAGly [10 µM]	1 µM [83]	5.0 ± 3.9	–	–	–
ADORA2B	0.6 ± 0.2; 8.79 ± 0.88	Bay [5.8 µM]	580 nM [84]	2.7 ± 2.7	–	–	–
P2RY11	0.3 ± 0.1; –	NF 546 [5.0 µM]	500 nM [85]	1.1 ± 1.1	–	–	–

Table 2: Human OPC-expressed $G\alpha_q$-coupled receptors differentially regulated oscillatory intracellular calcium fluctuations. RNA-seq data from human and mouse [62] was used to identify $G\alpha_q$-coupled receptors expressed by OPCs. FPKM values shown (mean ± SEM, n = 2). Ligands activating each receptor were identified to determine the calcium response characteristics in hOPCs. hOPCs were infected with GCaMP6s-expressing virus and exposed to various $G\alpha_q$-coupled receptor ligands at doses approximately 10-fold larger than reported EC_{50} values (or previously effective doses in rodent OPCs*). Calcium responses were recorded at least 10 minutes and analyzed as described. The percentage of responding cells, maximum response amplitude (fold), duration of response above baseline (minutes) and percentage of responding cells displaying an oscillatory calcium response was determined. While

$G\alpha_q$-coupled LPA receptors LPAR1 and LPAR4 were detected in hOPCs, due to the lack of specific ligands we did not test these receptors.

Abbreviations: **TRAP-6**, Thrombin receptor activating peptide 6; **TC-G**, 4-Methoxy-*N*-[[[2-trifluoromethyl)[1,1'-biphenyl]-4-yl]amino]carbonyl]-3-pyridinecarboxamide; **ET-1**, Endothelin-1; **PF9**, 2-(Phenylethynyl)adenosine-5'-triphosphate tetrasodium salt; **5-HT**, 5-hydroxytryptamine; **Oxo-M**, Oxotremorine methiodide; **CHPG**, 2-Chloro-5-hydroxyphenylglycine sodium salt; **2-PED**, 2-pyridylethylamide dihydrochloride; **NF 546**, 4,4'-(Carbonyl*bis*(imino-3,1-phenylene-carbonylimino-3,1-(4-methyl-phenylene)carbonylimino))-*bis*(1,3-xylene-alpha,alpha'-diphosphonic acid; **Bay**, Bay 60-6583, 2-[[6-Amino-3,5-dicyano-4-[4-cyclopropylmethoxy phenyl]-2-pyridinyl]thio]-acetamide; **MRS 2365**, [[(1*R*,2*R*,3*S*,4*R*,5*S*)-4-[6-Amino-2-(methylthio)-9*H*-purin-9-yl]-2,3-dihydroxybicyclo[3.1.0]hex-1yl]methyl] diphosphoric acid mono ester trisodium salt; **NAGly**, N-Arachidonoylglycine; **2-FLY**, 2-furoy-Leu-Ile-Gly-Arg-Leu-Orn-NH_2.

FIGURE LEGENDS

Figure 1. $G\alpha_q$-receptor activation induces ER-Ca^{2+} responses and SOCE in primary human OPC. Primary fetal brain-derived PDGFαR$^+$ hOPCs were infected with intracellular Ca^{2+} reporter GCaMP6s expressing lentivirus. Time-lapse microscopy of GCaMP6s fluorescence following $G\alpha_q$-receptor agonist treatment was recorded and analyzed. Dose response curves following treatment with either oxotremorine–M (Oxo-M) or CHPG illustrating the percentage of hOPCs responding to $G\alpha_q$ ligand treatment (**A, B**) and overall area under the curve (AUC) for $[Ca^{2+}]_i$ release per cell (**C, D**). Mean ± SEM shown of > 250 total cells per dose (n=3 human samples)**.** EC_{50} for AUC was calculated by non-linear regression for each compound. **E**, to directly assess SOCE GCaMP6s-expressing hOPCs were cultured in calcium-free conditions for 15 mins. Time-lapse microscopy was begun prior to treatment with thapsigargin (Tg) or Oxo-M (red dashed lines), followed by re-addition calcium to the culture media to stimulate SOCE (green dashed lines) in the presence (middle and bottom traces) or absence (top trace) of SOCE antagonists. Representative traces from three biological replicates showing mean pixel intensity per cell AUC ± SEM (blue shading). **F**, quantification of SOCE was performed by normalizing calcium influx to ER-depletion. Data are presented as mean ± SEM of ≥ 70 cells per each condition, n = 3 human samples. * p<0.05, one-way ANOVA with Holm-Sidak post-hoc test.

Figure 2. STIM1/2 calcium sensors are required for muscarinic-induced SOCE and $[Ca^{2+}]_i$ response in human OPCs. hOPCs were transfected with STIM1 and/or STIM2, or scrambled siRNA, cultured in mitogen-containing media, and RNA was extracted after 24-48 hours. For calcium imaging experiments, hOPCs were initially infected with GCaMP6s lentivirus and then transfected with STIM RNAi prior to time-lapse microscopy. Real-time quantitative PCR of STIM1 (**A)** or STIM2 (**B**) mRNA relative to scrambled control hOPCs following STIM1, STIM2 or STIM1/2 RNAi knockdown (STIM KD) (mean ± SEM, n=8 human samples). **C**, representative pseudo-colored fluorescence time-lapse images of peak Oxo-M-induced calcium responses in siRNA transfected hOPCs cultured in calcium-free conditions. Images represent peak Oxo-M [25μM] induced ER-store depletion (red text and arrows in **C** and **D** respectively) and SOCE following calcium re-addition (green text and arrows in **C** and **D** respectively). **D**, representative calcium traces of Oxo-M induced calcium response following siRNA transfection (mean ± SEM normalized AUC, SEM shown using blue shading, n ≥ 30 cells per condition). **E**, quantification of SOCE (AUC Influx/Depletion). STIM KD resulted in a substantial reduction in muscarinic-induced SOCE relative to control hOPCs. mean ± SEM of > 140 cells per condition, n=4 human samples. * p<0.05, ** p<0.01, *** p <0.001, ****p<0.0001, RM one-way ANOVA with Tukey's post-hoc test. **F–G**, the net effect of pharmacological SOCE inhibition or STIM KD on calcium Oxo-M-induced increased $[Ca^{2+}]_i$ was determined in calcium-containing media by time-lapse microscopy. STIM1 KD or STIM2 KD hOPCs

displayed a reduction in Oxo-M-induced calcium responses as denoted by reduced average AUC (**F**) as well as a reduction in oscillatory frequency relative to control hOPCs (**G**). Log transformed mean AUC ± SD of ≥ 100 cells per condition, n=4 independent human samples. * $p<0.05$, ** $p<0.01$, *** $p<0.001$, ****$p<0.0001$, one-way ANOVA with Dunnett's post-hoc t-tests. Scale: 50 µm.

Figure 3. Calcium sensor STIM2 regulates human OPC differentiation and is required for the anti-differentiative effect of muscarinic agonists. hOPCs were transfected with STIM1 and/or STIM2 siRNA, or control non-targeting siRNA, and 24 h later PDGF-AA and NT-3 were removed to induce oligodendrocyte differentiation. **A**, representative images of immature $O4^+$ oligodendrocytes (green) in the presence or absence of muscarinic agonist, Oxo-M [40µM]. **B**, quantification of the percentage of $O4^+$ oligodendrocyte differentiation among $DAPI^+$ cells (blue). Mean ± SEM shown (n=4 human samples). * $p<0.05$, ** $p<0.01$, O4% analyzed by three-way ANOVA with pairwise Holm-Sidak's post-hoc tests. **C**, the percentage of dividing OPCs defined as $KI\text{-}67^+/DAPI^+$ cells following siRNA transfection was determined in each group (n = 3 human samples). Both Oxo-M and STIM2 siRNA treatment resulted in a significantly decreased $O4^+$ oligodendrocyte differentiation ($p = 0.032$ and 0.0128, respectively). Importantly, Oxo-M treatment did not influence differentiation in the context of STIM1 knockdown ($p = 0.24$). STIM1/2 siRNA nor Oxo-M treatment significantly influenced OPC proliferation (three-way ANOVA, main effect $p > 0.05$). Scale: 50 µm.

Figure 4. OptoSTIM drives oscillatory calcium responses in hOPCs in the absence of $G\alpha_q$-coupled signaling. hOPCs were infected with OptoSTIM and jRCaMP1a lentiviruses to induce SOCE and observe calcium responses simultaneously. Cells were cultured in a temperature/CO_2 controlled chamber during time-lapse fluorescence microscopy. Blue light (488nm) excitation was used to induce SOCE at distinct frequencies (5 m or 30 m intervals, respectively) while intermittently probing for increases in jRCaMP1a fluorescence every 20 seconds. **A**, representative integrated calcium response to OptoSTIM-induced SOCE in the absence of $G\alpha_q$-receptor activation (n = 3 human samples). Images shown represent total fluorescence for 2.5 minutes before and after first stimulation. Exposure times were matched to ensure an equivalent amount of blue light stimulation across conditions (330 and 2000 ms per stimulus, respectively). **B**, representative traces of mean ± SEM normalized calcium response to varying frequencies over the course of 2.5 hours following a 30m baseline with no stimulation. SOCE was robustly induced throughout the imaging period and directly corresponded with the timing of blue light stimulation (vertical lines in middle and lower traces). **C**, quantification of integrated calcium responses at different stimulation frequencies measured for the duration of the stimulation period. Mean

± SEM of >50 cells per condition (n=3 human samples). * $p<0.05$, RM one-way ANOVA with Tukey's post-hoc test. Scale: 50 µm.

Figure 5. SOCE is sufficient to block hOPC differentiation and promote hOPC mitosis. Matched cultures of primary hOPCs were infected with OptoSTIM lentivirus and imaged for 2-3 days in an on-stage temperature/CO_2 controlled chamber. Bright field images were acquired every 5 minutes. OptoSTIM-mediated SOCE was induced with intermittent 488nm excitation (5m or 30m interval for 330ms and 2000ms duration, respectively). **A**, hOPC proliferation was quantified by counting mitotic events (white arrowheads). **B**, the cumulative proportion of cells undergoing mitosis was quantified over 36 h following the onset of blue light stimulation. **C,** proliferation rates were normalized to the matched unstimulated condition. High frequency (3.33 mHz) OptoSTIM induction of SOCE resulted in a significant increase in hOPC mitotic events compared to control unstimulated and low frequency (0.55 mHz) stimulated hOPCs. **D**, the effect of OptoSTIM-induced SOCE on hOPC differentiation was determined by O4 immunocytochemistry (red) at 48 hrs post-stimulation. OptoSTIM transduced cells were identified by GFP expression which was uniform across experimental conditions (**E**). **F**, quantification of $O4^+$ oligodendrocyte differentiation following OptoSTIM-induced SOCE (% $O4^+/GFP^+$). **G**, analysis of $O4^+$ morphological maturation. High frequency (3.33 mHz) SOCE induced a significant reduction in $O4^+$ cells as well as a significant reduction in complex branching morphology relative to control hOPCs. * $p<0.05$, RM one-way ANOVA with Tukey's post-hoc tests. Mean ± SEM shown for each panel (n=4 human samples). Scale: 25 µm.

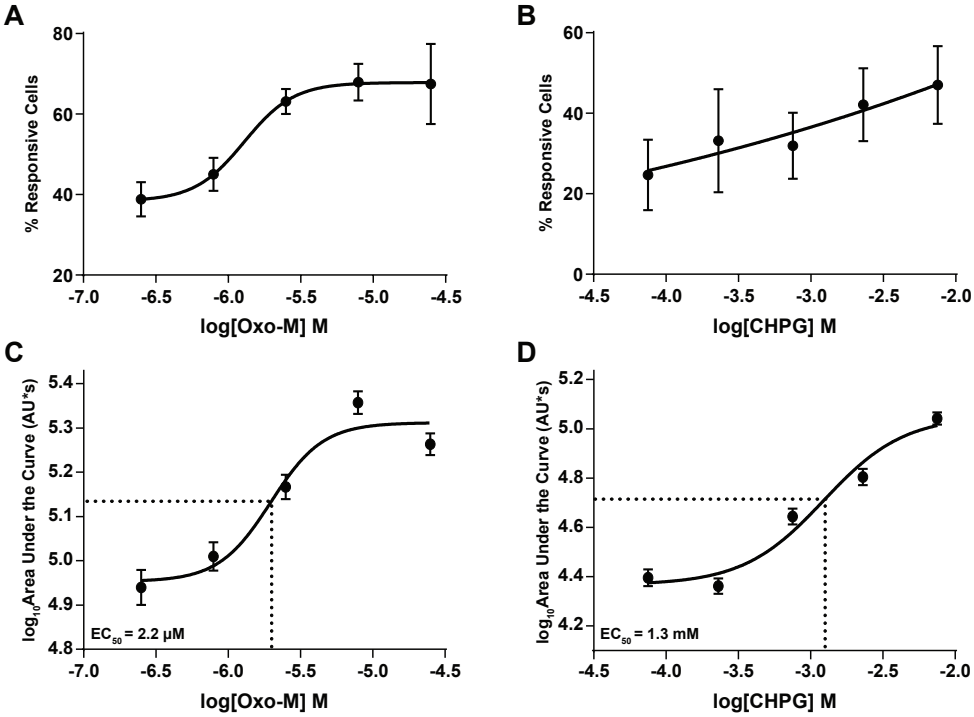
A
% Responsive Cells
log[Oxo-M] M
B
% Responsive Cells
log[CHPG] M
C
log10Area Under the Curve (AU*s)
EC50 = 2.2 μM
log[Oxo-M] M
D
log10Area Under the Curve (AU*s)
EC50 = 1.3 mM
log[CHPG] M

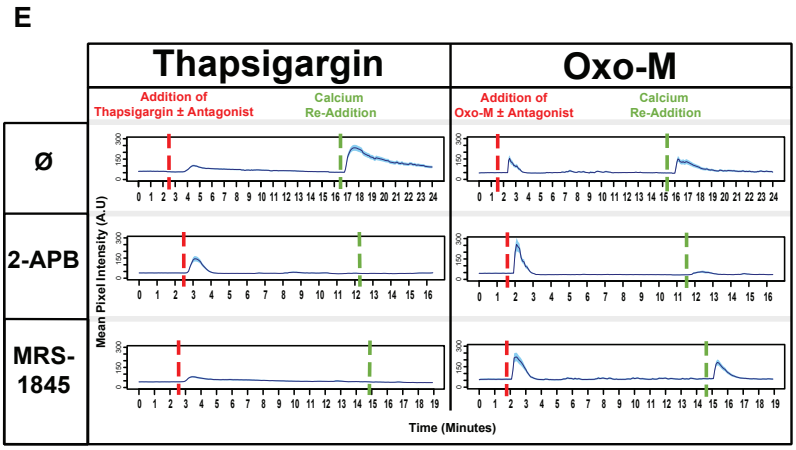
E
Thapsigargin
Oxo-M
Addition of Thapsigargin ± Antagonist
Calcium Re-Addition
Addition of Oxo-M ± Antagonist
Calcium Re-Addition
Ø
2-APB
MRS-1845
Mean Pixel Intensity (A.U)
Time (Minutes)

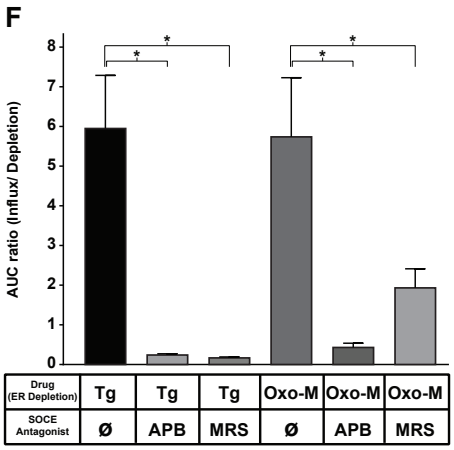
F
AUC ratio (Influx/ Depletion)
Drug (ER Depletion)
Tg
Tg
Tg
Oxo-M
Oxo-M
Oxo-M
SOCE Antagonist
Ø
APB
MRS
Ø
APB
MRS

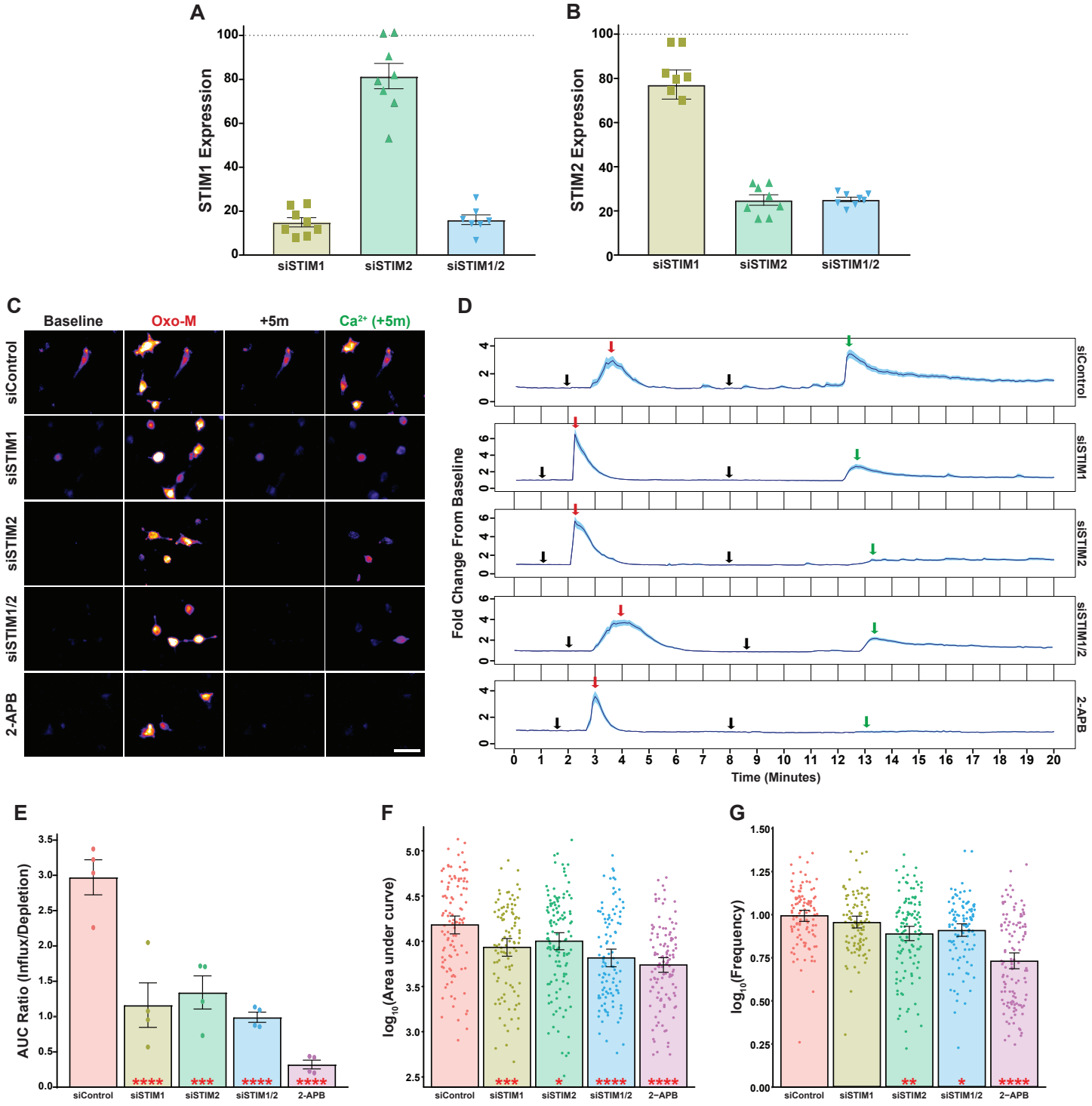
A
STIM1 Expression
siSTIM1
siSTIM2
siSTIM1/2
B
STIM2 Expression
siSTIM1
siSTIM2
siSTIM1/2
C
Baseline
Oxo-M
+5m
Ca2+ (+5m)
siControl
siSTIM1
siSTIM2
siSTIM1/2
2-APB
D
Fold Change From Baseline
Time (Minutes)
siControl
siSTIM1
siSTIM2
siSTIM1/2
2-APB
E
AUC Ratio (Influx/Depletion)
siControl
siSTIM1
siSTIM2
siSTIM1/2
2-APB
F
log10(Area under curve)
siControl
siSTIM1
siSTIM2
siSTIM1/2
2-APB
G
log10(Frequency)
siControl
siSTIM1
siSTIM2
siSTIM1/2
2-APB

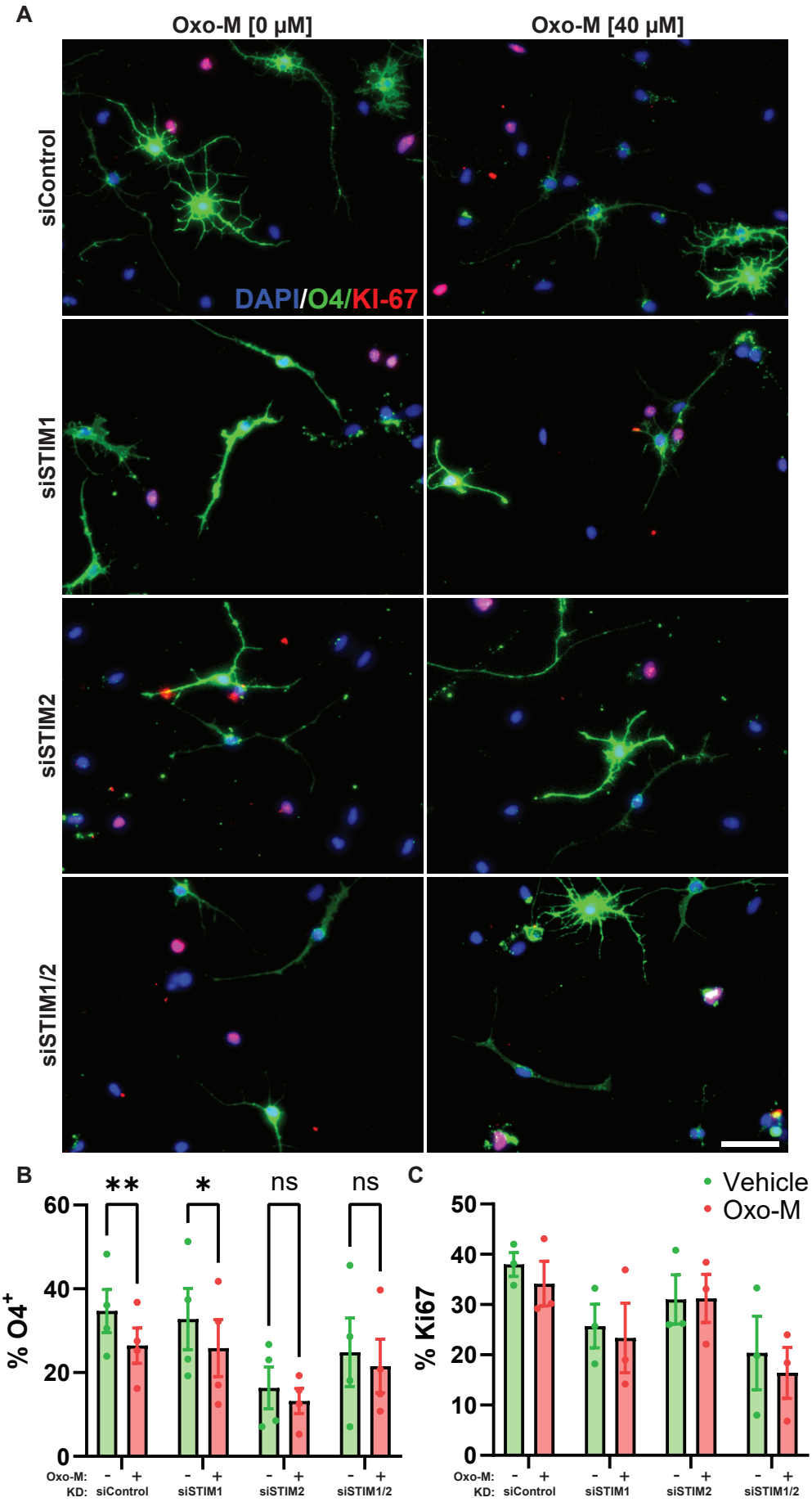
A
Oxo-M [0 μM]
Oxo-M [40 μM]
siControl
siSTIM1
siSTIM2
siSTIM1/2
DAPI/O4/KI-67
B
**
*
ns
ns
% O4+
60
40
20
0
Oxo-M: - + - + - + - +
KD: siControl siSTIM1 siSTIM2 siSTIM1/2
C
Vehicle
Oxo-M
% Ki67
50
40
30
20
10
0
Oxo-M: - + - + - + - +
KD: siControl siSTIM1 siSTIM2 siSTIM1/2

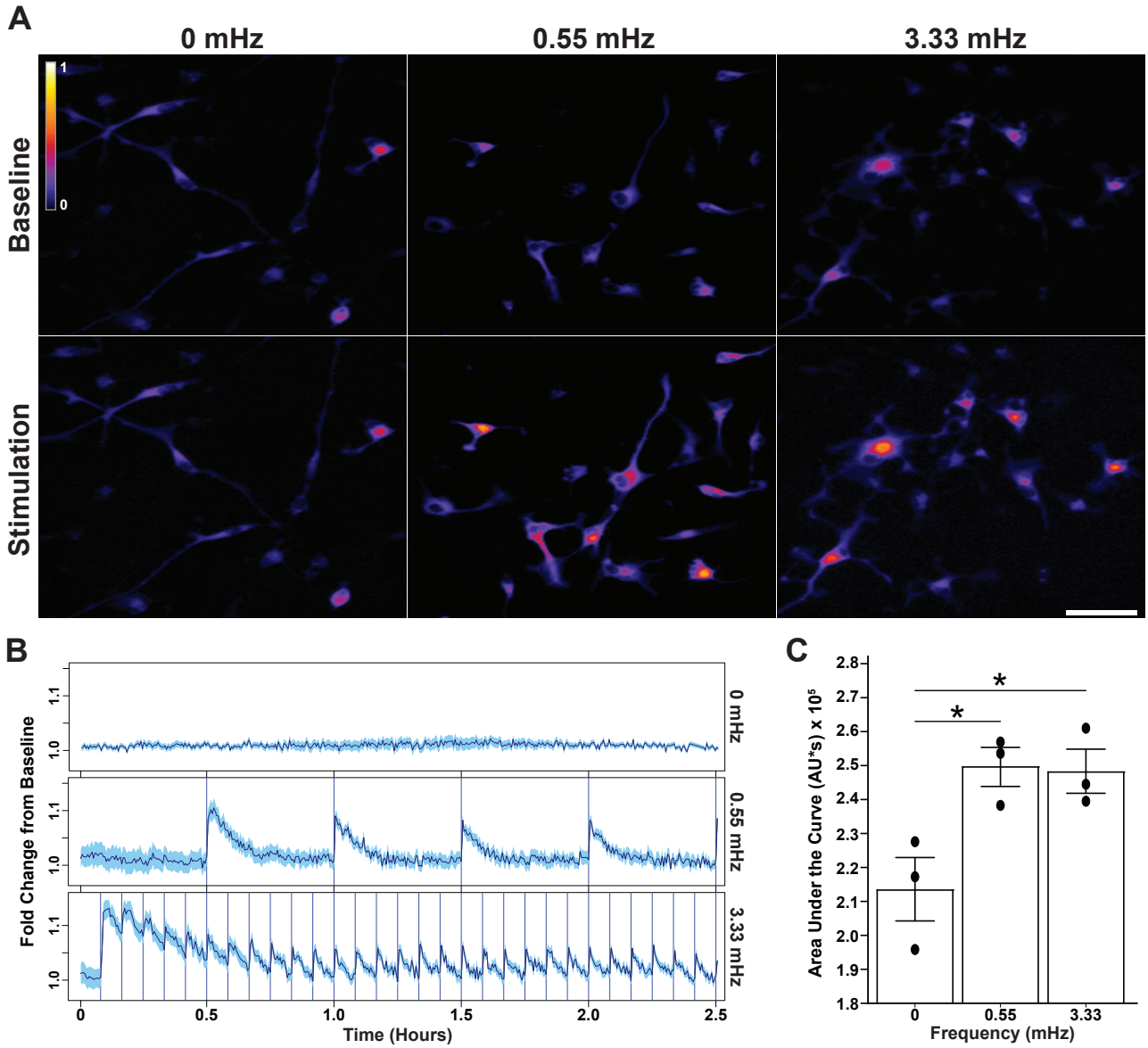
A
0 mHz
0.55 mHz
3.33 mHz
Baseline
Stimulation
1
0
B
Fold Change from Baseline
1.1
1.0
0 mHz
0.55 mHz
3.33 mHz
0
0.5
1.0
1.5
2.0
2.5
Time (Hours)
C
Area Under the Curve (AU*s) x 10^5
2.8
2.7
2.6
2.5
2.4
2.3
2.2
2.1
2.0
1.9
1.8
*
*
0
0.55
3.33
Frequency (mHz)

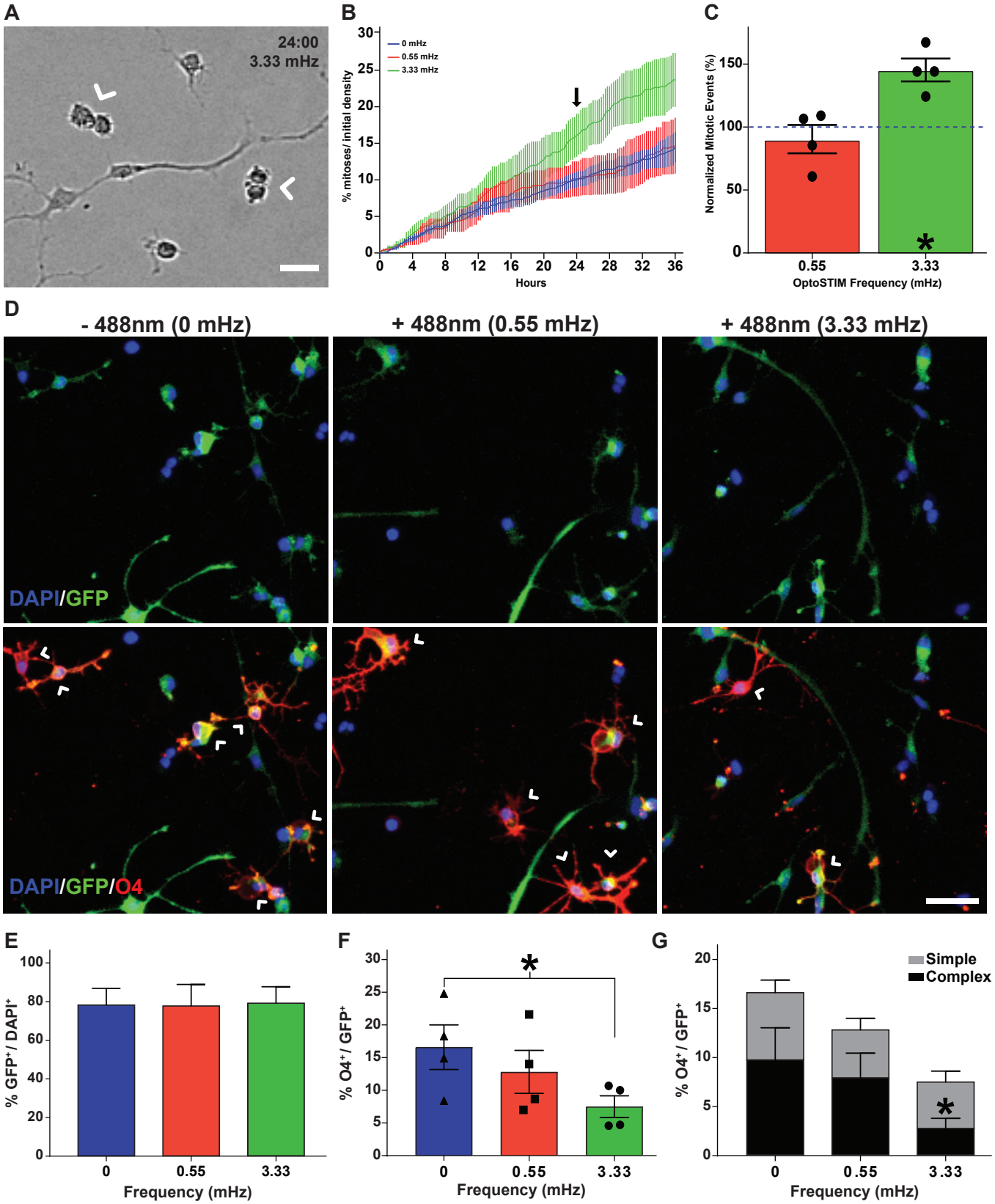
A
24:00
3.33 mHz
B
0 mHz
0.55 mHz
3.33 mHz
% mitoses/ initial density
Hours
C
Normalized Mitotic Events (%)
OptoSTIM Frequency (mHz)
D
- 488nm (0 mHz)
+ 488nm (0.55 mHz)
+ 488nm (3.33 mHz)
DAPI/GFP
DAPI/GFP/O4
E
% GFP+ / DAPI+
Frequency (mHz)
F
% O4+ / GFP+
Frequency (mHz)
G
Simple
Complex
% O4+ / GFP+
Frequency (mHz)

Extended Data Figure Legends

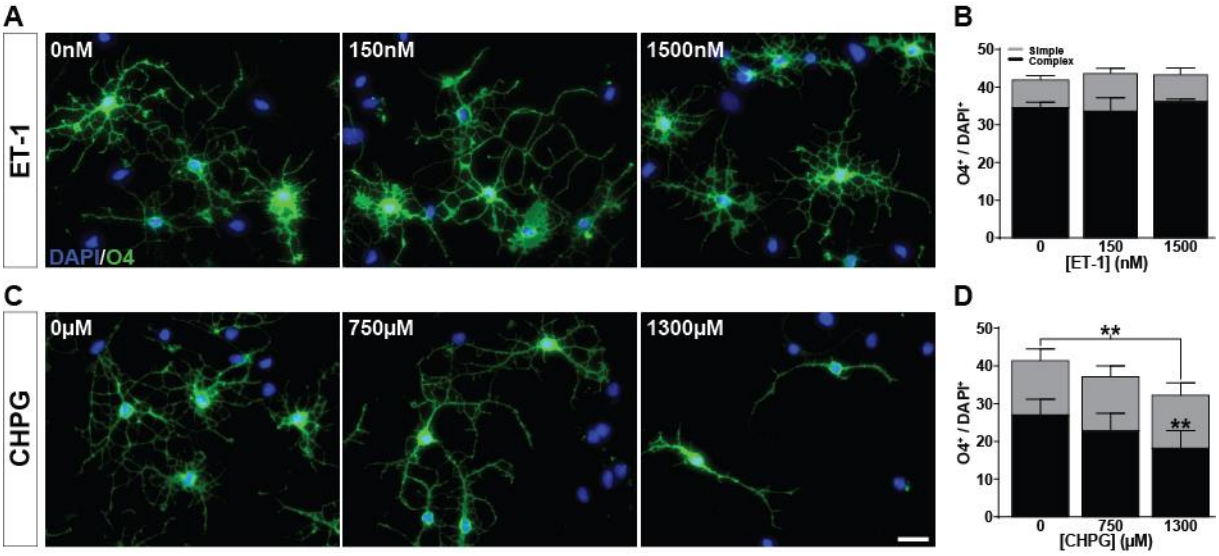

Figure 1-1 (related to Figure 1). mGluR5 activation attenuates hOPC differentiation. The effects of various G_q receptor ligands on hOPC differentiation was assessed *in vitro*. **A**, following removal of mitogens, hOPCs were treated with ET-1 to activate endothelin-B receptor (0 - 1500nM). The effect of ET-1 on oligodendrocyte differentiation was determined by quantification of immature $O4^+$ oligodendrocytes (green). **B,** quantification of morphologically simple (< 3 primary processes) and complex $O4^+$ oligodendrocytes (mean ± SEM, n = 2 individual fetal samples). ET-1 stimulation did not influence $O4^+$ oligodendrocyte differentiation. **C**, treatment with $mGluR_5$ agonist CHPG (0 - 1300 μM) significantly reduced $O4^+$ oligodendrocyte differentiation and morphologically mature complex $O4^+$ cells (**quantified in D**, mean ± SEM, n = 5 individual fetal samples). ** $p<0.01$, RM one-way ANOVA with Tukey's post-hoc test. Scale: 25 μm.

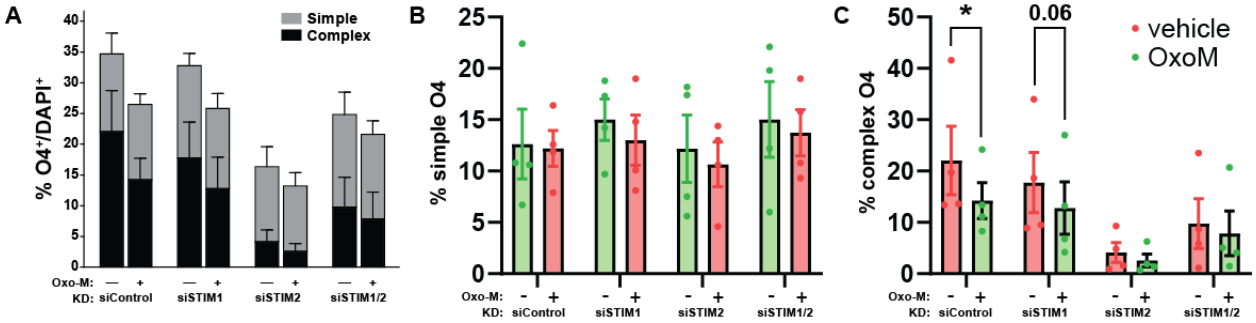

Figure 3-1 (related to Figure 3). Effect of STIM1/2 siRNA treatment of human oligodendrocyte morphological maturation. Morphological maturation of $O4^+$ oligodendrocytes was assessed by determining the proportion of complex branching and simple process bearing cells. $O4^+$ oligodendrocytes were characterized as complex if they had at least 3 highly branched processes. **A**, quantification of both simple and complex O4+ oligodendrocytes. Mean ± SEM shown (n=4 fetal samples). **B**, analysis of simple $O4^+$ oligodendrocytes. Three-way ANOVA indicates that STIM1 or STIM2 do not influence the percentage of O4+ oligodendrocytes (main effects, $p > 0.3$). In contrast, OxoM treatment has a highly significant effect on simple O4+ percentage ($p = 0.0068$). **C**, analysis of complex $O4^+$ oligodendrocytes. Three-way ANOVA revealed a significant effect of STIM2 siRNA on complex $O4^+$ cells. * indicates $p < 0.05$ Holm-Sidak posthoc test relative to control. Following STIM1 or STIM2 siRNA treatment, OxoM did not significantly influence the proportion of complex $O4^+$ cells.